Corpora non agunt nisi fixata : ligand receptor binding kinetics in G protein-coupled receptors

Xia, L.

Chapter 3

Kinetics of human Cannabinoid 1 (CB_1) receptor antagonists: structure-kinetics relationships (SKRs) and implications for insurmountable antagonism

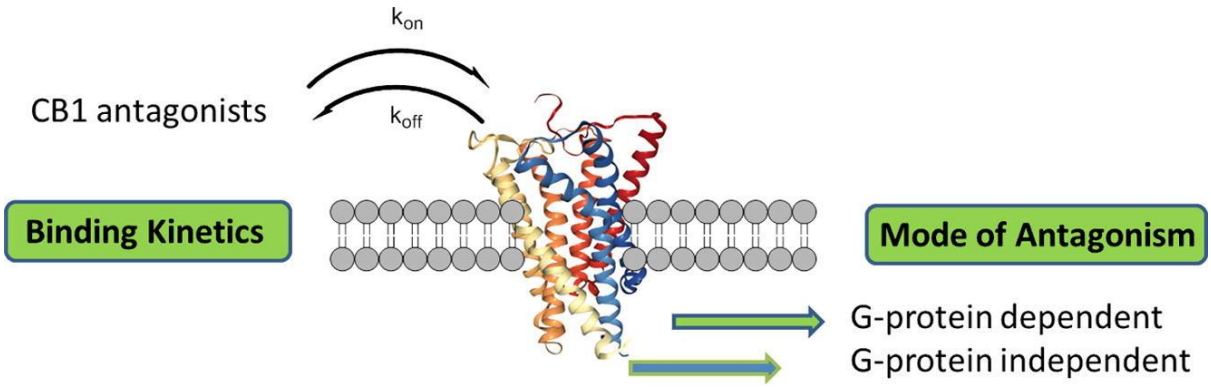

Binding kinetics of CB1 antagonists defines their mode of functional antagonism

Lizi Xia, Henk de Vries, Xue Yang, Eelke B. Lenselink, Athina Kyrizaki, Francis Barth, Julien Louvel, Matthias K. Dreyer, Daan van der Es, Adriaan P. IJzerman, Laura H. Heitman

Adapted from: *Biochem. Pharmacol.* **2017** doi: 10.1016/j.bcp.2017.10.014. [Epub ahead of print]

About this chapter

While equilibrium binding affinities and *in vitro* functional antagonism of human CB_1 receptor antagonists have been studied in detail, little is known on the kinetics of their receptor interaction. In this study, we therefore conducted kinetic assays for nine 1-(4,5-diarylthiophene-2-carbonyl)-4-phenylpiperidine-4-carboxamide derivatives and included the CB_1 antagonist rimonabant as a comparison. For this we newly developed a dual-point competition association assay with [^{3}H]CP55940 as the radioligand. This assay yielded Kinetic Rate Index (KRI) values from which structure-kinetics relationships (SKR) of hCB_1 receptor antagonists could be established. The fast dissociating antagonist **6** had a similar receptor residence time (RT) as rimonabant, i.e. 19 and 14 min, respectively, while the slowest dissociating antagonist (**9**) had a very long RT of 2222 min, i.e. pseudo-irreversible dissociation kinetics. In functional assays, **9** displayed insurmountable antagonism, while the effects of the shortest RT antagonist **6** and rimonabant were surmountable. Taken together, this study shows that hCB_1 receptor antagonists can have very divergent RTs, which are not correlated to their equilibrium affinities. Furthermore, their RTs appear to define their mode of functional antagonism, i.e. surmountable vs. insurmountable. Finally, based on the recently resolved hCB_1 receptor crystal structure, we propose that the differences in RT can be explained by a different binding mode of antagonist **9** from short RT antagonists that is able to displace unfavorable water molecules. Taken together, these findings are of importance for future design and evaluation of potent and safe hCB_1 receptor antagonists.

Introduction

The human cannabinoid 1 (hCB_1) receptor is categorized as a "lipid G protein-coupled receptor (GPCR)" due to its hydrophobic endogenous ligands, such as anandamide (AEA) and 2-arachidonoylglycerol (2-AG), which are crucial components of the endocannabinoid system (ECS).[1, 2] The CB_1 receptor belongs to the class A GPCR family, and has been shown to signal through inhibitory $G_{\alpha i/o}$ heterotrimeric G proteins,[3] and to interact with β-arrestin.[4] Nowadays, it is widely acknowledged that the hCB_1 receptor is not only present in the central nervous system (CNS), but also widely distributed in the peripheral nervous system (PNS) and peripheral tissues,[5] including the heart, lung, liver, gastrointestinal tract, pancreas and adipose tissue.[6, 7] The ECS, including the hCB_1 receptor, has been shown to be overactive in metabolic disorders where increased endocannabinoid levels are found in plasma, in central and peripheral tissues.[8] Therefore, blockade of the hCB_1 receptor is seen as a potential approach for the treatment of metabolic disorders such as obese dyslipidemia, liver disease and diabetes.[9]

Rimonabant, as an anti-obesity drug, was the first hCB_1 receptor antagonist to reach the market in Europe, but was withdrawn in 2008 by the manufacturer because of the risk of serious psychiatric adverse effects, such as depression.[10-13] As a result, many research programs in this field were terminated. Afterwards, the development of peripherally-restricted hCB_1 antagonists gained attention, as they may not have CNS-related side-effects. The general strategy was to introduce more polar or even ionic functional groups to a ligand's scaffold. However, some recent clinical and pre-clinical reports on this type of compounds either show no antiobesity effect at all [14] or no improved effect in comparison to rimonabant.[14-17]

Most recently, the concept of drug target binding kinetics is receiving increased attention. In particular the receptor-ligand residence time (RT) is emerging as an additional parameter to assess the therapeutic potential of drug candidates with respect to drug efficacy and safety.[18-20] The strategic combination of structure-kinetic relationship (SKR) with classic structure-affinity

relationship (SAR) analyses results in a better understanding of a ligand-receptor interaction, as together this not only comprises the equilibrium state of a ligand-receptor interaction but also its metastable intermediates and/or transition states. Recently, a number of structure-kinetic relationship (SKR) studies have been published in the field of GPCR.[21-24] These suggest that including binding kinetic data when triaging compounds can change, and hopefully improve, the resulting decision process as a compound's target affinity and residence time are not always correlated.

In the current study, a series of 9 previously reported peripherally-selective 1-(4,5-diarylthiophene-2-carbonyl)-4-phenylpiperidine-4-carboxamide derivatives were selected for a structure-kinetics relationships (SKR) study, next to structure-affinity relationships (SAR). These compounds arose from so-called scaffold hopping, where the pyrazole ring of rimonabant was replaced by a five-membered thiophene ring.[25, 26] In addition, some polar substituents were introduced on the thiophene and phenyl rings, as well as a carboxamide moiety; all to increase the ligands' polar surface area, and thus to reduce brain penetration (**Table 1**). Together with rimonabant as a reference, they were evaluated in equilibrium and kinetic radioligand binding assays yielding affinity values and kinetic binding parameters, which resulted in traditional SAR and novel SKR, respectively. All compounds had high affinities, but possessed diverse kinetic profiles at the hCB_1 receptor. This "kinetic screening campaign" led to the identification of a very long (**9,** 2222 min) and short RT hCB_1 receptor antagonist (**6,** 19 min), while rimonabant was determined to have a RT of 14 min. Subsequently, we applied two other radioligand binding experiments (i.e. "two-step incubation" and "wash-out" equilibrium displacement experiments) to characterize the pseudo-irreversible binding kinetics of antagonist **9**, compared to the reversible binding kinetics of antagonist **6** and rimonabant. With such large differences in RT (~185 fold), we decided to further investigate their concomitant functional effects in both G protein-dependent and -independent (i.e. β-arrestin recruitment) signaling. Their putative binding mode was analyzed using the recently resolved crystal structures of the hCB_1 receptor,[27] shedding light on key structural features of the receptor binding site that are involved in dissociation or pseudo-irreversible binding. In summary, we provide evidence that, next to affinity,

additional knowledge of a compound's binding kinetics is useful for selecting and developing new and, potentially, improved hCB_1 receptor antagonists in the early phases of drug discovery.

Method

Chemicals and reagents. The syntheses of antagonists **1**-**9** have been described previously.[25, 26] All compounds were fully characterized by HPLC and ^{1}H NMR. For compounds **1**, **2**, **3**, **4**, **8** and **9**, purity was analyzed by a Symmetry C18 column (50 x 2.1 mm ; 3.5 µm), with a 15 minute gradient of acetonitrile/water (0 % -> 90 % CH_3CN). For compound **5**, purity was analyzed by an XTerra MS C18 column (50 x 2.1 mm ; 3.5 µm), with a 15 minute gradient of acetonitrile/10mM ammonium acetate with 3% CH_3CN (0 % -> 90 % CH_3CN). For compound **6** and **7**, purity was analyzed by an Acquity BEH C18 column (50 x 2.1 mm ; 1.7 µm), with a 3 minute gradient of acetonitrile/water with 3% CH_3CN (1 % -> 95 % CH_3CN). All antagonists were found to have a purity of 95% or higher. The compound characterization details for the nine antagonists are shown below.

*1-[[5-(2,4-Dichlorophenyl)-4-[4-(2-hydroxyethoxy)phenyl]-2-thienyl]carbonyl]-4-phenyl-4-piperidinecarboxamide (**1**).* ^{1}H NMR (600 MHz, DMSO-d_6) δ 7.72 (s, 1H), 7.59 (s, 1H), 7.48 (s, 2H), 7.43 (d, J = 7.6 Hz, 2H), 7.35 (t, J = 7.7 Hz, 2H), 7.28 – 7.22 (m, 2H), 7.14 – 7.08 (m, 3H), 6.85 (d, J = 8.8 Hz, 2H), 4.83 (t, J = 5.5 Hz, 1H), 4.15 (d, J = 12.5 Hz, 2H), 3.94 (t, J = 4.9 Hz, 2H), 3.68 (q, J = 5.2 Hz, 2H), 2.54 (d, J = 8.7 Hz, 2H), 1.89 (t, J = 10.7 Hz, 2H). Purity: 99%. Retention Time: 9.26 min.

*1-[[4-[4-[(2-Aminoethyl)thio]phenyl]-5-(2,4-dichlorophenyl)-2-thienyl]carbonyl]-4-phenyl-4-piperidinecarboxamide (**2**).* ^{1}H NMR (600 MHz, DMSO-d_6) δ 7.88 (bs, 3H), 7.75 (d, J = 1.8 Hz, 1H), 7.64 (s, 1H), 7.54 – 7.48 (m, 2H), 7.42 (d, J = 7.4 Hz, 2H), 7.36 (t, J = 7.8 Hz, 2H), 7.30 (d, J = 8.5 Hz, 2H), 7.25 (t, J = 7.3 Hz, 2H), 7.19 (d, J = 8.4 Hz, 2H), 7.11 (s, 1H), 4.15 (d, J = 11.2 Hz, 2H), 3.17 (t, J = 7.3 Hz, 2H), 2.95 (t, J = 7.3 Hz, 2H), 2.55 (d, J = 14.1 Hz, 2H), 1.96 – 1.83 (m, 2H). Purity: 99 %. Retention Time: 7.34 min.

*1-[[5-(2,4-Dichlorophenyl)-4-[4-[[2-[(methylsulfonyl)amino]ethyl]thio]phenyl]-2-thienyl]carbonyl]-4-phenyl-4-piperidinecarboxamide (**3**).* ^{1}H NMR (600 MHz, DMSO-d_6) δ 7.74 (d, *J* = 1.3 Hz, 1H), 7.65 (s, 1H), 7.54 – 7.47 (m, 2H), 7.43 (d, *J* = 7.4 Hz, 2H), 7.35 (t, *J* = 7.8 Hz, 2H), 7.27 (s, 1H), 7.25 (d, *J* = 4.5 Hz, 4H), 7.16 (d, *J* = 8.5 Hz, 2H), 7.10 (s, 1H), 4.16 (d, *J* = 12.6 Hz, 2H), 3.15 – 3.10 (m, 2H), 3.10 – 3.03 (m, 2H), 2.89 (s, 3H), 2.55 (d, *J* = 13.5 Hz, 2H), 1.89 (t, *J* = 10.6 Hz, 2H). Purity: 100 %. Retention Time: 9.79 min.

*1-[[5-(2,4-Dichlorophenyl)-4-[4-[3-(methylsulfonyl)propoxy]phenyl]-2-thienyl]carbonyl]-4-phenyl-4-piperidinecarboxamide (**4**).* ^{1}H NMR (600 MHz, DMSO-d_6) δ 7.73 (s, 1H), 7.60 (s, 1H), 7.48 (d, *J* = 1.0 Hz, 2H), 7.42 (d, *J* = 7.4 Hz, 2H), 7.35 (t, *J* = 7.8 Hz, 2H), 7.28 – 7.22 (m, 2H), 7.13 (d, *J* = 8.8 Hz, 2H), 7.10 (s, 1H), 6.86 (d, *J* = 8.8 Hz, 2H), 4.16 (d, *J* = 14.0 Hz, 2H), 4.05 (t, *J* = 6.2 Hz, 2H), 3.26 – 3.22 (m, 2H), 3.00 (sz, 3H), 2.55 (d, *J* = 13.6 Hz, 2H), 2.16 – 2.07 (m, 2H), 1.89 (t, *J* = 11.2 Hz, 2H). Purity: 95 %. Retention Time: 9.64 min.

*1-[[5-(2,4-Dichlorophenyl)-4-[4-[(3-hydroxypropyl)thio]phenyl]-2-thienyl]carbonyl]-4-phenyl-4-piperidinecarboxamide (**5**).* ^{1}H NMR (600 MHz, DMSO-d_6) δ 7.73 (d, *J* = 0.9 Hz, 1H), 7.63 (s, 1H), 7.49 (d, *J* = 1.7 Hz, 2H), 7.42 (d, *J* = 7.4 Hz, 2H), 7.36 (t, *J* = 7.8 Hz, 2H), 7.25 (t, *J* = 7.2 Hz, 2H), 7.21 (d, *J* = 8.5 Hz, 2H), 7.14 (d, *J* = 8.5 Hz, 2H), 7.10 (s, 1H), 4.55 (t, *J* = 5.2 Hz, 1H), 4.15 (d, *J* = 13.4 Hz, 2H), 3.47 (q, *J* = 6.0 Hz, 2H), 2.98 (t, *J* = 7.3 Hz, 2H), 2.57 – 2.52 (m, 2H), 1.89 (t, *J* = 12.4 Hz, 2H), 1.69 (p, *J* = 6.6 Hz, 2H). Purity: 100 %. Retention Time: 9.28 min.

*1-[[5-(2,4-Dichlorophenyl)-4-[4-[(3-hydroxypropyl)sulfonyl]phenyl]-2-thienyl]carbonyl]-4-phenyl-4-piperidinecarboxamide (**6**).* ^{1}H NMR (600 MHz, DMSO-d_6) δ 7.81 (d, *J* = 8.4 Hz, 2H), 7.76 – 7.73 (m, 2H), 7.55 (d, *J* = 8.3 Hz, 1H), 7.52 (dd, *J* = 8.3, 2.0 Hz, 1H), 7.48 (d, *J* = 8.5 Hz, 2H), 7.43 (d, *J* = 7.5 Hz, 2H), 7.36 (t, *J* = 7.8 Hz, 2H), 7.25 (t, *J* = 7.2 Hz, 2H), 7.10 (s, 1H), 4.63 (t, *J* = 5.3 Hz, 1H), 4.17 (d, *J* = 13.3 Hz, 2H), 3.40 (q, *J* = 6.0 Hz, 2H), 3.30 – 3.24 (m, 2H), 2.54 (d, *J* = 14.2 Hz, 2H), 1.90 (t, *J* = 12.3 Hz, 2H), 1.70 – 1.60 (m, 2H). Purity: 100 %. Retention Time: 1.52 min.

*1-[[5-(2,4-Dichlorophenyl)-4-[4-[(4-hydroxybutyl)thio]phenyl]-2-thienyl]carbonyl]-4-phenyl-4-piperidinecarboxamide (**7**).* ^{1}H NMR (600 MHz, DMSO-d_6) δ 7.73 (d, J = 0.8 Hz, 1H), 7.64 (s, 1H), 7.52 – 7.47 (m, 2H), 7.43 (d, J = 7.5 Hz, 2H), 7.36 (t, J = 7.8 Hz, 2H), 7.26 (t, J = 7.2 Hz, 2H), 7.21 (d, J = 8.4 Hz, 2H), 7.14 (d, J = 8.4 Hz, 2H), 7.11 (s, 1H), 4.42 (t, J = 5.1 Hz, 1H), 4.16 (d, J = 13.3 Hz, 2H), 2.95 (t, J = 7.2 Hz, 2H), 2.54 (d, J = 15.6 Hz, 2H), 1.90 (t, J = 12.6 Hz, 2H), 1.63 – 1.56 (m, 2H), 1.55 – 1.49 (m, 2H). Purity: 100 %. Retention Time: 1.79 min.

*4-[5-[(4-Carbamoyl-4-phenylpiperidin-1-yl)carbonyl]-2-(2,4-dichlorophenyl)thien-3-yl]phenyl propane-1-sulfonate (**8**).* ^{1}H NMR (600 MHz, DMSO-d_6) δ 7.74 (d, J = 2.0 Hz, 1H), 7.68 (s, 1H), 7.51 (dt, J = 8.3, 5.2 Hz, 2H), 7.43 (d, J = 7.4 Hz, 2H), 7.36 (t, J = 7.8 Hz, 2H), 7.33 – 7.29 (m, 2H), 7.29 – 7.23 (m, 4H), 7.11 (s, 1H), 4.16 (d, J = 13.3 Hz, 2H), 3.56 – 3.46 (m, 2H), 2.54 (d, J = 14.0 Hz, 2H), 1.90 (t, J = 12.2 Hz, 2H), 1.86 – 1.78 (m, 2H), 1.02 (t, J = 7.4 Hz, 3H). Purity: 98 %. Retention Time: 10.62 min.

*1-[[5-(2,4-Dichlorophenyl)-4-[4-[3-(methylthio)propoxy]phenyl]-2-thienyl]carbonyl]-4-phenyl-4-piperidinecarboxamide (**9**).* ^{1}H NMR (600 MHz, DMSO-d_6) δ 7.72 (s, 1H), 7.59 (s, 1H), 7.48 (d, J = 1.0 Hz, 2H), 7.43 (d, J = 7.4 Hz, 2H), 7.36 (t, J = 7.8 Hz, 2H), 7.25 (t, J = 7.2 Hz, 2H), 7.17 – 7.07 (m, 3H), 6.85 (d, J = 8.8 Hz, 2H), 4.15 (d, J = 12.2 Hz, 2H), 4.01 (t, J = 6.1 Hz, 2H), 2.59 (t, J = 7.2 Hz, 2H), 2.54 (d, J = 13.1 Hz, 2H), 2.05 (s, 3H), 1.97 – 1.91 (m, 2H), 1.91 – 1.83 (m, 2H). Purity: 98 %. Retention Time: 11.43 min.

[^{3}H]CP55940 (specific activity 141.2 Ci/mmol) and [^{35}S]GTPγS (specific activity 1250 Ci/mmol) were purchased from Perkin Elmer (Waltham, MA). Bicinchoninic acid (BCA) and BCA protein assay reagent was obtained from Pierce Chemical Company (Rochford, IL). Rimonabant (SR141716A) was from Cayman Chemical Company (Ann Arbor, MI). CHOK1hCB1_bgal and CHOK1hCB2_bgal cells (catalog number 93-0959C2 and 93-0706C2) and the Pathhunter® detection kit (catalog number 93-0001M) were obtained from DiscoveRx (Fremont, CA). All other chemicals were of analytical grade and obtained from standard commercial sources.

Cell culture and membrane preparation. CHOK1hCB1_bgal cells and CHOK1hCB2_bgal cells were cultured in Ham's F12 Nutrient Mixture supplemented with 10% fetal calf serum (FCS), 1 mM glutamine, 50 μg/ml penicillin, 50 μg/ml streptomycin, 300 mg/ml hygromycin and 800 μg/ml geneticin in a humidified atmosphere at 37°C and 5% CO_2. Cells were subcultured twice a week at a ratio of 1:10 on 10-cm ø plates by trypsinization. For membrane preparation the cells were subcultured 1:10 and transferred to large 15 cm ø plates. Membrane fractions were prepared as described before.[28]

Radioligand equilibrium displacement assays. Membrane aliquots containing 5 μg (CHOK1hCB1_bgal) or 1.5 μg (CHOK1hCB2_bgal) protein were incubated in a total volume of 100 μL assay buffer (50 mM Tris–HCl, 5 mM $MgCl_2$, 0.1% BSA, pH 7.4) at 30°C for 60 min. Displacement experiments were performed using 6 concentrations of competing antagonist in the presence of a final concentration of ~3 nM [^{3}H]CP55940 (CHOK1hCB1_bgal) or ~1.5 nM [^{3}H]CP55940 (CHOK1hCB2_bgal). At this concentration, total radioligand binding did not exceed 10% of that added to prevent ligand depletion. Nonspecific binding (NSB) was determined in the presence of 10 μM rimonabant (CHOK1hCB1_bgal) or 10 μM AM630 (CHOK1hCB2_bgal). For the "two-step incubation" assays, antagonists were first pre-incubated with membrane aliquots at 30 °C for 3 h, then ~3 nM of [^{3}H]CP55940 was added and coincubated for a further 60 min. For all experiments, incubation was terminated by rapid filtration performed on 96-well GF/C filter plates (Perkin Elmer, Groningen, the Netherlands), presoaked for 30 min with 0.25% PEI (PolyethyleneImine), using a PerkinElmer Filtermate-harvester (Perkin Elmer, Groningen, the Netherlands). After drying the filter plate at 50 °C for 30 min, the filter-bound radioactivity was determined by scintillation spectrometry using the 2450 MicroBeta^2 Plate Counter (Perkin Elmer, Boston, MA).

"Wash-out" assays. For washout experiments, 100 μl assay buffer containing either 1% DMSO (as blank control for total binding and non-specific binding) or antagonist (**9**, **6** or rimonabant, final concentration 1 μM stock in assay buffer) was added to 1.5-ml Eppendorf tubes containing 20 μg of

CHOK1hCB1_bgal protein. This mixture was brought to a total volume of 300 µL assay buffer, which was then incubated at 30 °C for 1 h. Subsequently, the mixture was centrifuged at 13,000 revolutions per minute (RPM) at 4 °C for 5 min to allow the removal of the supernatant containing unbound ligand. Then the membrane pellet was resuspended in 1 ml assay buffer by vortexing and spun at 13,000 RPM at 4 °C for 10 min. After three washing cycles, the membrane pellets were resuspended in 300 µl assay buffer and placed on ice. Subsequently, 100 µl [^{3}H] CP55940 (~3 nM) was added, followed by another incubation at 30 °C for 60 min. Incubation was terminated by rapid filtration performed on GF/C filters (Whatman International, Maidstone, UK), presoaked for 30 min with 0.25% PEI, using a Brandel harvester (Brandel, Gaithersburg, MD). Filter-bound radioactivity was determined by scintillation spectrometry using a Tri-Carb 2900 TR liquid scintillation counter (Perkin Elmer, Boston, MA).

Radioligand association and dissociation assays. Association experiments were performed by incubating membrane aliquots containing 5 µg of CHOK1hCB1_bgal membrane in a total volume of 100 µL of assay buffer at 30 °C with ~3 nM [^{3}H]CP55940. The amount of radioligand bound to the receptor was measured at different time intervals during a total incubation of 120 min. Dissociation experiments were performed by preincubating membrane aliquots containing 5 µg of protein in a total volume of 100 µL of assay buffer for 60 min. After the preincubation, radioligand dissociation was initiated by the addition of 5 µl 10 µM unlabeled rimonabant. The amount of radioligand still bound to the receptor was measured at various time intervals for a total of 240 min to ensure that full dissociation from hCB_1 receptor was reached. Incubations were terminated and samples were obtained as described under *Radioligand equilibrium displacement assays.*

Radioligand competition association assays. The binding kinetics of unlabeled ligands were quantified using the competition association assay based on the theoretical framework by Motulsky and Mahan.[29] The competition association assay was initiated by adding membrane aliquots (5 µg/well) at different time points for a total of 240 min to a total volume of 100 µl of assay buffer at

30 °C with ~3 nM [^{3}H]CP55940 in the absence or presence of a single concentration of competing hCB_1 receptor antagonists (1 to 3-fold IC_{50}). Incubations were terminated and samples were obtained as described under *Radioligand equilibrium displacement assays.* The "dual-point" competition association assays were designed as described previously,[30] where in this case the two time points were selected at 30 (t_1) and 240 min (t_2).

*[^{35}S]GTPγS binding assays for selected long and short RT antagonists (**9, 6,** rimonabant).* The assays were performed by incubating 5 µg of homogenized CHOK1CB1_bgal membranes in a total volume of 80 µl assay buffer (50 mM Tris-HCl buffer, 5 mM $MgCl_2$, 150 mM NaCl, 1 mM EDTA, 0.05% BSA and 1 mM DTT, pH 7.4) supplemented with 1 µM GDP and 5 µg saponin. The assays were performed in a 96-well plate format, where DMSO stock solutions of the compounds were added using a HP D300 Digital Dispenser (Tecan, Männedorf, Switserland). The final concentration of organic solvent per assay point was ≤0.1%. In all cases, the basal level of [^{35}S]GTPγS binding was measured in untreated membrane samples, whereas the maximal level of [^{35}S]GTPγS binding was measured by treatment of the membranes with 1 µM CP55940, unless stated otherwise. To determine the IC_{50} values (inverse agonism) of hCB_1 receptor antagonists, as well as EC_{50} values of CP55940 (a reference CB_1 receptor agonist), the membranes were incubated with increasing concentrations of ligand for 90 minutes at 30°C. To determine the IC_{50} (antagonism) values of hCB_1 receptor antagonists, membrane preparations were pre-incubated for 30 min at 30 °C with a range of concentrations of the antagonists prior to the addition of an EC_{80} concentration of CP55940 (3.8 nM) and 20 µL [^{35}S]GTPγS (final concentration ~0.3 nM) after which incubation continued for another 90 min at 30 °C. For the insurmountability experiments, membrane preparations were pre-incubated with or without antagonists (10-, 30-, 100-fold K_i values) for 60 min at 30 °C, prior to the addition of CP55940 (1 µM to 0.1 nM) and 20 µl [^{35}S]GTPγS (final concentration ~0.3 nM), after which incubation continued for another 30 min at 30 °C. For the surmountability (control) experiments, antagonists and CP55940 were co-incubated with [^{35}S]GTPγS for 30 min at 30 °C. For all experiments, incubations were

terminated and samples were obtained as described under *Radioligand equilibrium displacement assays,* by using GF/B filters (Whatman International, Maidstone, UK).

PathHunter® β*-arrestin recruitment assays for selected long and short RT antagonists (**9, 6,** rimonabant).* The PathHunter® protein complementation assay (Fremont, CA, USA) was performed according to the manufacturer's protocol.[31] CHOK1hCB1_bgal cells were seeded at a density of 5,000 cells per well of solid black-walled 384-well plates (Catalogue number 3712, Corning, NY, USA) in 20 µl cell culture medium and incubated overnight in a humidified atmosphere at 37 °C and 5% CO_2. DMSO stock solutions of the compounds were added using a HP D300 Digital Dispenser (Tecan, Männedorf, Switzerland). The final concentration of organic solvent per assay point was ≤0.1 %. The basal level of β-arrestin recruitment was measured in untreated cells, and the maximal level of β-arrestin recruitment was measured by treatment of cells with 1 µM CP55940, unless stated otherwise. To determine the IC_{50} values (inverse agonism) of hCB_1 receptor antagonists, as well as EC_{50} values of CP55940, the cells were stimulated with increasing concentrations of ligand and incubated for 90 min (standard duration) or 6 h (extended duration) in a humidified atmosphere at 37 °C and 5 % CO_2. To determine the IC_{50} (inhibition) values of hCB_1 receptor antagonists, the cells were exposed to increasing concentrations of each antagonist and preincubated for 30 min under the same condition, followed by the addition of an EC_{80} concentration of CP55940 (39 nM), after which the cells were incubated for 90 min in a humidified atmosphere at 37 °C and 5% CO_2. For the insurmountability assays, the cells were pre-incubated with or without antagonists (10-, 30-, 100-fold K_i values on the hCB_1 receptor) for 60 min, after that CP55940 (1 µM to 0.1 nM) was added and incubated for another 30 min. For the surmountability (control) experiments, antagonists and CP55940 were co-incubated for 30 min at 37 °C and 5% CO_2. For all the experiments, β-galactosidase enzyme activity was determined by using the PathHunter® detection mixture, according to the kit's protocol.[31] Detection mixture (12 µL per well) was added and the plate was incubated for 60 min in the dark at room temperature. Chemiluminescence, indicated as relative light units (RLU), was measured on an EnVision multilabel plate reader (Perkin Elmer, MA, USA).

*Computational studies on selected long and short RT antagonists (**9, 6,** rimonabant).* The computational studies were based on the crystal structure of the hCB_1 receptor co-crystalized with AM6538 (PDB: 5TGZ) [27] and prepared with the protein preparation wizard.[32] Since the antagonists **9**, **6** and rimonabant were similar to the co-crystalized AM6538, induced fit docking [33] was used with core constraints on the 2,4-dichlorophenyl ring of AM6538. To study to the potential differences in hydration between ligands, an apo (without ligand present) WaterMap was generated.[34, 35] Figures were rendered using PyMol,[36] for clarity the "cartoon" representation of residues 362 to 375 was hidden.

Data analysis. All experimental data were analyzed using the nonlinear regression curve fitting program GraphPad Prism 6.0 (GraphPad Software, Inc., San Diego, CA). From displacement assays, IC_{50} values were obtained by non-linear regression analysis of the displacement curves. The obtained IC_{50} values were converted into K_i values using the Cheng-Prusoff equation to determine the affinity of the ligands,[37] using a K_D value of 0.10 nM (CHOK1hCB1_bgal) and 0.33 nM (CHOK1hCB2_bgal).[38] The observed association rates (k_{obs}) derived from both assays were obtained by fitting association data using 'one phase exponential association'. The dissociation rate constants were obtained by fitting dissociation data to a 'one phase exponential decay' model. The k_{obs} values were converted into association rate constants (k_{on}) using the equation $k_{on} = (k_{obs} – k_{off})/[L]$, where [L] is the amount of radioligand used for the association experiments. The association and dissociation rate constants were used to calculate the kinetic K_D using the equation $K_D = k_{off}/k_{on}$. The residence time (RT, in min) was calculated using the equation $RT = 1/(60 * k_{off})$, as k_{off} is in s^{-1}. Association and dissociation rate constants for unlabeled compounds were calculated by fitting the data into the competition association model using "kinetics of competitive binding":[29]

$$K_A = k_1[L]\cdot 10^{-9} + k_2$$

$$K_B = k_3[I]\cdot 10^{-9} + k_4$$

$$S = \sqrt{(K_A - K_B)^2 + 4\cdot k_1 \cdot k_3 \cdot L \cdot I \cdot 10^{-18}}$$

$$K_F = 0.5(K_A + K_B + S)$$

$$K_S = 0.5(K_A + K_B - S)$$

$$Q = \frac{B_{\max} \cdot k_1 \cdot L \cdot 10^{-9}}{K_F - K_S}$$

$$Y = Q \cdot \left(\frac{k_4 \cdot (K_F - K_S)}{K_F \cdot K_S} + \frac{k_4 - K_F}{K_F} e^{(-K_F \cdot X)} - \frac{k_4 - K_S}{K_S} e^{(-K_S \cdot X)}\right)$$

where k_1 is the k_{on} of the radioligand ($M^{-1}s^{-1}$), k_2 is the k_{off} of the radioligand (s^{-1}), L is the radioligand concentration (nM), I is the concentration of the unlabeled competitor (nM), X is the time (s) and Y is the specific binding of the radioligand (DPM). The control curve (without competitor) from competition association assays generated the k_1 value, and the k_2 value was obtained in previous experiments (data not shown). With that the k_3, k_4 and B_{max} were calculated, where k_3 represents the k_{on} ($M^{-1}s^{-1}$) of the unlabeled ligand, k_4 stands for the k_{off} (s^{-1}) of the unlabeled ligand and B_{max} equals the total binding (DPM). All competition association data were globally fitted. [^{35}S]GTPγS binding and β-arrestin recruitment curves were analyzed by nonlinear regression using "log (agonist or inhibitor) vs response-variable slope" to obtain potency, inhibitory potency or efficacy values of agonists and inverse agonists (EC_{50}, IC_{50} or E_{max}, respectively). In the (in)surmountability assays, Gaddum/Schild EC_{50} shift equations were used to obtain Schild-slopes and *p*A_2 values; statistical analysis with two-way ANOVA with Tukey's post-test was applied. All values obtained are means of at least three independent experiments performed in duplicate, unless stated otherwise.

Results

Binding affinity (K_i) of hCB$_1$ receptor antagonists.

Table 1. Equilibrium binding affinity (K_i) and kinetic parameters (KRI, k_{on}, k_{off}, RT and K_D) for hCB_1 receptor antagonists

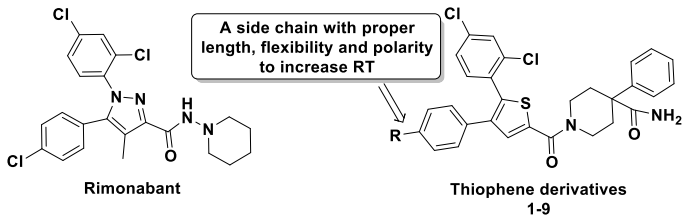

Antagonist	R	CB_1 binding						CB_2 binding
		pKi ± SEM (K_i in nM)[a]	KRI [b]	k_{on} [c] ($M^{-1}s^{-1}$)	k_{off} [d] (s^{-1})	RT [e] (min)	K_D [f] (nM)	pKi ± SEM (K_i in nM)[g]
Rimonabant	N.A.[h]	8.8 ± 0.1 (1.8)	0.65 ± 0.03	(2.3 ± 0.3) x 10^5	(1.4 ± 0.2) x 10^{-3}	14 ± 2.0	5.9 ± 0.3	N.D.[i]
1	$-OCH_2CH_2OH$	9.3 ± 0.1 (0.53)	0.81 ± 0.02	N.D.	N.D.	N.D.	N.D.	7.7 ± 0.1 (22)
2	$-SCH_2CH_2NH_2$	9.3 ± 0.04 (0.53)	1.30 ± 0.21	N.D.	N.D.	N.D.	N.D.	7.8 ± 0.5 (33)
3	$-SCH_2CH_2NHSO_2CH_3$	9.7 ± 0.03 (0.19)	1.39 (1.41; 1.36)	(1.5 ± 0.2) x 10^5	(3.0 ± 0.7) x 10^{-5}	556 ± 124	0.22 ± 0.07	8.8 ± 0.04 (1.6)
4	$-OCH_2CH_2CH_2SO_2CH_3$	9.3 ± 0.1 (0.50)	1.08 (1.10; 1.06)	N.D.	N.D.	N.D.	N.D.	7.3 ± 0.1 (58)
5	$-SCH_2CH_2CH_2OH$	9.6 ± 0.1 (0.28)	1.02 ± 0.31	N.D.	N.D.	N.D.	N.D.	8.2 ± 0.3 (9.7)
6	$-SO_2CH_2CH_2CH_2OH$	7.9 ± 0.01 (14)	0.70 ± 0.17	(5.2 ± 0.7) x 10^4	(8.8 ± 1.7) x 10^{-4}	19 ± 3.6	18 ± 3.1	7.2 ± 0.1 (74)
7	$-SCH_2CH_2CH_2CH_2OH$	9.6 ± 0.1 (0.24)	1.32 ± 0.15	(1.4 ± 0.2) x 10^5	(4.7 ± 0.7) x 10^{-5}	357 ± 51	0.34 ± 0.02	7.6 ± 0.1 (26)
8	$-OSO_2CH_2CH_2CH_3$	9.9 ± 0.03 (0.13)	1.51 ± 0.14	(2.0 ± 0.2) x 10^5	(3.8 ± 1.2) x 10^{-5}	435 ± 132	0.19 ±0.05	7.4 ± 0.02 (38)
9	$-OCH_2CH_2CH_2SCH_3$	8.9 ± 0.1 (1.4)	1.57 ± 0.39	(8.5 ± 0.8) x 10^4	(7.5 ± 3.0) x 10^{-6}	2222 ± 888	0.084 ± 0.026	7.3 ± 0.1 (54)

[a] pK_i ± SEM (n = 3), obtained from radioligand binding assays with [^{3}H] CP55940 on recombinant human CB_1 receptors stably expressed on CHO cell membranes.

[b] KRI ± SEM (n = 3) or KRI (n_1; n_2) (n = 2), obtained from dual-point competition association assays with [^{3}H] CP55940 on recombinant human CB_1 receptors stably expressed on CHO cell membranes.

[c] k_{on} ± SEM (n = 3), obtained from competition association assays with [^{3}H] CP55940 on recombinant human CB_1 receptors stably expressed on CHO cell membranes.

[d] k_{off} ± SEM (n = 3), obtained from competition association assays with [^{3}H] CP55940 on recombinant human CB_1 receptors stably expressed on CHO cell membranes.

[e] RT = 1/(60 * k_{off}); RT is expressed in min, whereas k_{off} is expressed in s-1.

[f] $K_D = k_{off}/k_{on}$.

[g] pK_i ± SEM (n = 3), obtained from radioligand binding assays with [^{3}H] CP55940 on recombinant human CB_2 receptors stably expressed on CHO cell membranes.

[h] N.A. not applicable.

[i] N.D. not determined.

The binding affinities of nine hCB_1 receptor antagonists were determined in equilibrium radioligand displacement studies. All antagonists were able to concentration-dependently inhibit specific [^{3}H]CP55940 binding to the human CB_1 receptor and their affinities are listed in **Table 1**. All antagonists had a high binding affinity, ranging from 0.13 nM for antagonist **8** to 14 nM for antagonist **6**, while the reference antagonist, rimonabant, had an affinity of 1.8 nM. Moreover, we determined the affinity of all nine compounds on the hCB_2 receptor. From **Table 1** it follows that they all had higher affinity for the hCB_1 receptor, where approximately 5-292-fold selectivity over hCB_2 receptors was observed.

Kinetic Rate Index (KRI) values of hCB_1 receptor antagonists.

Subsequently, these hCB_1 receptor antagonists were screened in the so-called "dual-point" competition association assay. The specific binding of [^{3}H]CP55940 was measured after 30 and 240 minutes in the absence and presence of a single concentration of unlabeled hCB_1 receptor antagonists, which yielded their Kinetic Rate Index (KRI). The KRI values of the hCB_1 receptor antagonists ranged from 0.65 to 1.57 (**Table 1**). Antagonists with a KRI value larger than 1.0 were considered to have a slower dissociation rate, and thus a longer RT, than the radioligand used, i.e.

[^{3}H]CP55940, and *vice versa.* Four antagonists (**3**, **7**, **8** and **9**) had KRI values ≥ 1.3, whereas two antagonists (**6** and rimonabant) had KRI values ≤ 0.7 (**Table 1**).

Structure−Affinity Relationships (SAR) and Structure−Kinetics Relationships (SKR) of hCB$_1$ receptor antagonists.

The obtained affinities (K_i values) and kinetic profiles (k_{on}, k_{off} values and RTs) permitted us to derive SAR and SKR for this series of antagonists. Different sidechains were examined as the R group (**Table 1**). On antagonist **1** the R_1 substituent was a 2-hydroxyethoxy, which resulted in a high affinity of 0.53 nM and a KRI-value of 0.81. When the side chain of antagonist **1** was replaced by a similar 2-mercaptoethylamine (**2**), its affinity was unchanged and its KRI value was substantially increased to 1.30. When the terminal amine of **2** was extended by methanesulfonyl ($-SO_2CH_3$) as in antagonist **3**, it yielded an approximately 3-fold increased affinity (0.53 nM vs 0.19 nM) and slightly higher KRI value (1.39). The slightly less polar side chain of antagonist **4** did not improve affinity in comparison to **2** but slightly reduced the KRI value (1.08). Next, a 3-mercapto-1-propanol side chain was introduced (**5**), which did not affect the affinity, but the compound's KRI value was close to unity (1.02). When the thio-ether of **5** was oxidized to sulfonyl (**6**), the affinity was decreased by 50-fold to 14 nM and the KRI value reduced to 0.70. When the propyl side chain of antagonist **5** was extended to a butyl (**7**), the affinity remained the same (0.28 nM vs. 0.24 nM), but its KRI value increased to 1.32. Lastly, antagonists **8** and **9** were obtained by slight variations of the linear side chains from antagonists **6** and **7**, respectively, which resulted in pronounced effects on both affinity and kinetics. From the 5-mercapto-1-pentanol side chain (**7**) to 3-(methylthio)propan-1-ol (**9**), the affinity dropped by approximately 6-fold (0.24 nM vs. 1.4 nM), while the KRI value increased from 1.32 to the highest of the series (1.57). From sulfonic 1-propanol (**6**) to alkyl sulfate (**8**), not only the affinity improved from 14 nM to 0.13 nM (107-fold), but also its KRI value increased from the lowest value of the series (0.70) to the second highest value (1.51, **Table 1**).

Binding kinetics of selected hCB$_1$ receptor antagonists using the competition association assay.

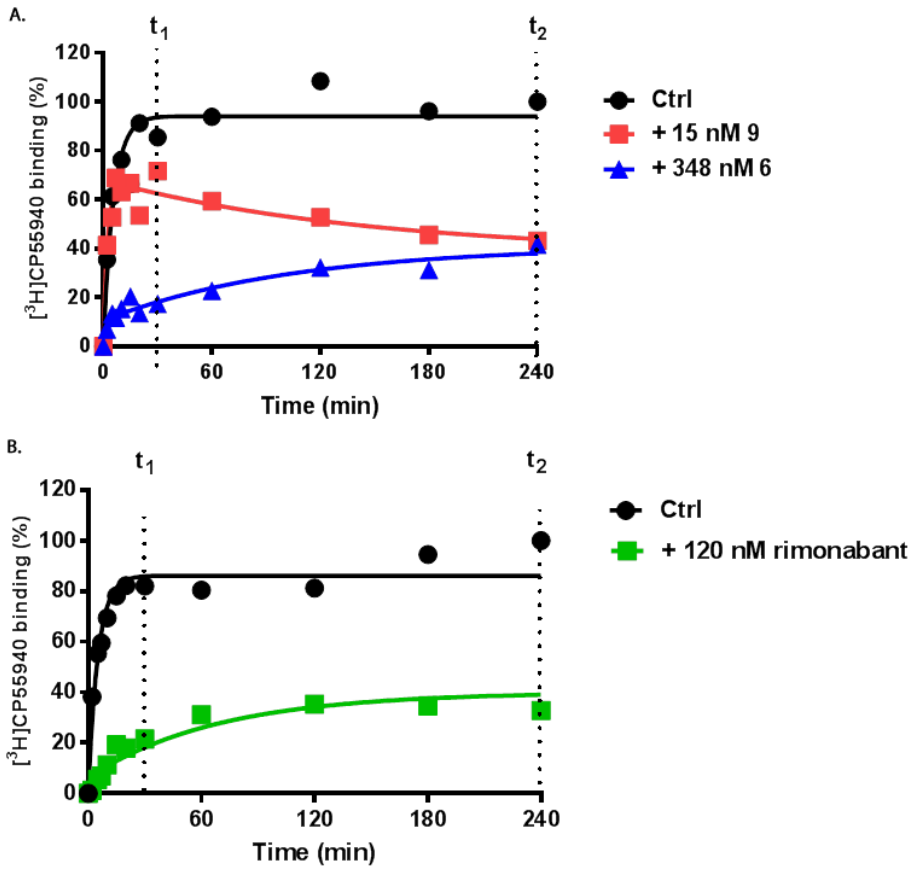

Figure 1. Competition association experiments with [^{3}H]CP55940 binding to recombinant hCB$_1$ receptors stably expressed on CHO cell membranes (30 °C) in the absence or presence of unlabeled long-residence-time antagonist **9** (**A**), short-residence-time antagonist **6** (**A**), or reference antagonist rimonabant (**B**). Representative graphs are shown from one experiment performed in duplicate. Note, t_1, t_2 are indicated, which were the two time points used in KRI determinations. Data are summarized in **Table 1**.

Next, the kinetic binding parameters of six antagonists that had either low or high KRI values (**3, 6, 7, 8, 9** and rimonabant) were determined using the competition association assay with [^{3}H]CP55940. Association rate constants varied by merely 4.5-fold, ranging from (5.2 ± 0.7) x 10^4 $M^{-1}s^{-1}$ for compound **6** to (2.3 ± 0.3) x 10^5 $M^{-1}s^{-1}$ for rimonabant (**Table 1**). There was a 180-fold difference in dissociation rate constants, in line with the divergent KRI values. Rimonabant had the fastest dissociation rate constant of (1.4 ± 0.2) x 10^{-3} s^{-1} and thus the shortest RT of 14 min, while compound **9** had the slowest dissociation rate constant of (7.5 ± 3.0) x 10^{-6} s^{-1} and thus the longest RT of 2222 min (**Table 1**). Of note, the long RT antagonist **9** (**Figure 1A**) displayed a typical "overshoot" in the association curve, indicative of a slower dissociation than [^{3}H]CP55940, while the short RT

antagonists, both antagonist **6** (**Figure 1A**) and rimonabant (**Figure 1B**), presented gradually ascending curves.

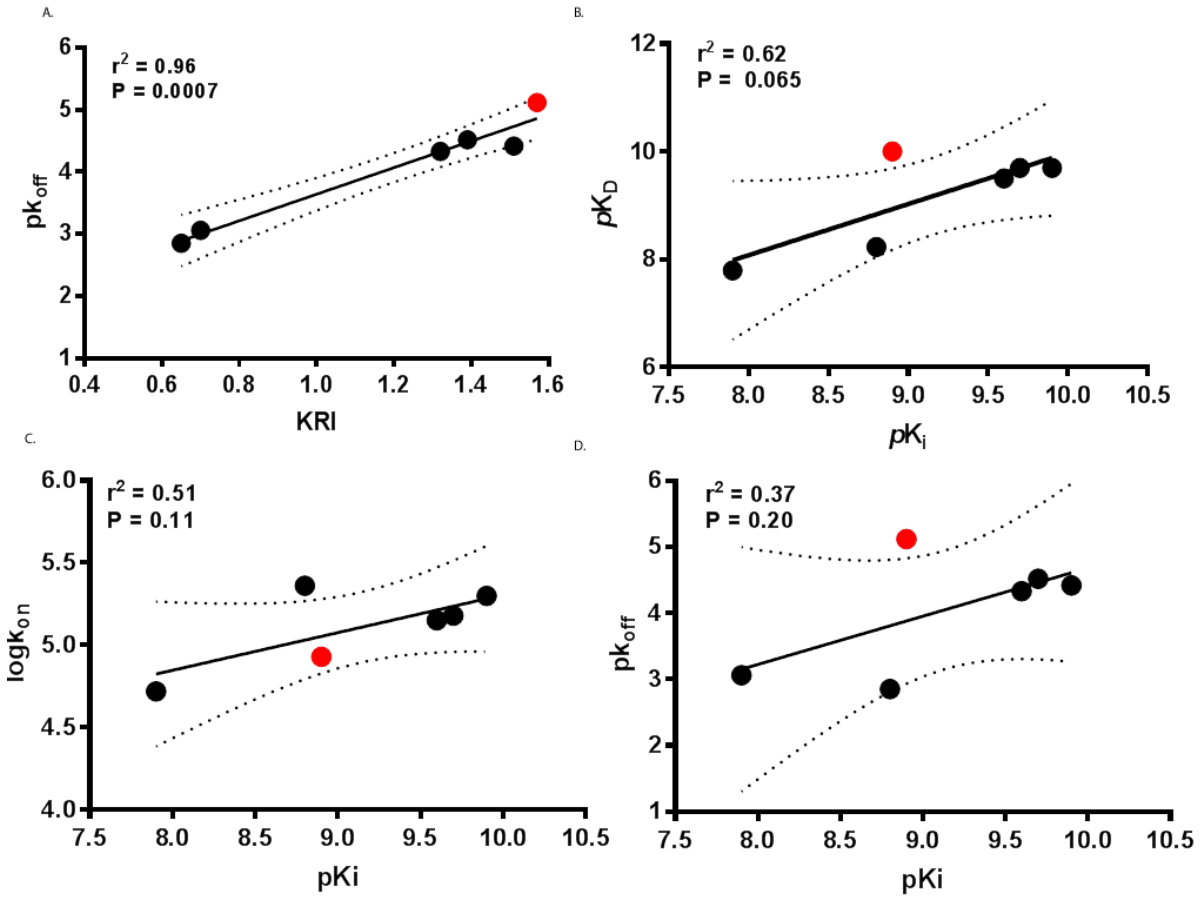

Figure 2. The correlations between the negative logarithm of the hCB$_1$ receptor antagonists' dissociation rate constants (pk$_{off}$) and their Kinetic Rate Index (KRI) (**A**), the CB$_1$ receptor antagonists' affinity (pK$_i$) and their "kinetic K$_D$" (pK$_D$) (**B**), association rate constants (log k$_{on}$) (**C**) and dissociation rate constants (pk$_{off}$) (**D**). The data point of the longest RT antagonist **9** is highlighted in red. Data used in these plots are detailed in **Table 1**. The central line corresponds to the linear regression of the data, the dotted lines represent the 95% confidence intervals for the regression.

Notably, a good correlation between the negative logarithm of the antagonist's dissociation rate constants and their KRI values derived from the kinetic assays was obtained (**Figure 2A**), which confirmed that a compound's KRI value is a good predictor for its dissociation rate constant. A significant correlation was also observed between the antagonist affinities (pK$_i$ values) determined in equilibrium displacement experiments and their pK$_D$ values derived from competition association

experiments (**Figure 2B**). In contrast, the kinetic parameters (log k_{on} or pk_{off} values) of the hCB_1R antagonists did not show a significant correlation with their affinities (**Figure 2C** and **2D**).

Binding kinetics of selected hCB_1 receptor antagonists using (pseudo-)equilibrium binding assays.

As another means to investigate differences in compound binding kinetics, "two-step incubation" equilibrium displacement experiments were performed for the long (**9**) and short RT antagonists (**6** and rimonabant), as shown in **Figure 3A**-**C**. When the displacement curves of the longest RT antagonist **9** were compared with the control and the two-step incubation, a significant one log-unit shift was observed (**Figure 3A**) resulting in a pK_i of 8.9 ± 0.1 to 9.8 ± 0.1, respectively. In contrast, no such affinity-shift was observed for either short RT antagonist (**Figure 3B** and **C, Table 2**), indicative of quick equilibration kinetics.

Table 2. Affinities of selected long (**9**) and short (**6**) RT hCB_1 receptor antagonists determined by the "two-step incubation" assays, using rimonabant as a reference.

Antagonists	"Two-step" incubation[a] (pK_i ± SEM)	Standard assay (Control)[b] (pK_i ± SEM)	"Affinity Shift"[c] (log unit)
9	9.8 ± 0.1 *	8.9 ± 0.1	+ 0.9
6	7.9 ± 0.04 ns	7.9 ± 0.01	0
Rimonabant	8.7 ± 0.1 ns	8.8 ± 0.1	- 0.1

[a] pK_i ± SEM (n = 3), obtained from radioligand binding assays with [^{3}H] CP55940 on recombinant human CB_1 receptors stably expressed on CHO cell membranes.

[b] pK_i ± SEM (n = 3), obtained from radioligand binding assays with [^{3}H] CP55940 on recombinant human CB_1 receptors stably expressed on CHO cell membranes (taken from **Table 1** for comparison).

[c] Affinity shift = pK_i (two-step incubation) - pK_i (standard assay).

Student's t-test was applied for the comparison of "affinity" obtained from "two-step" incubation by standard affinity, * $p < 0.05$, ns for not significant.

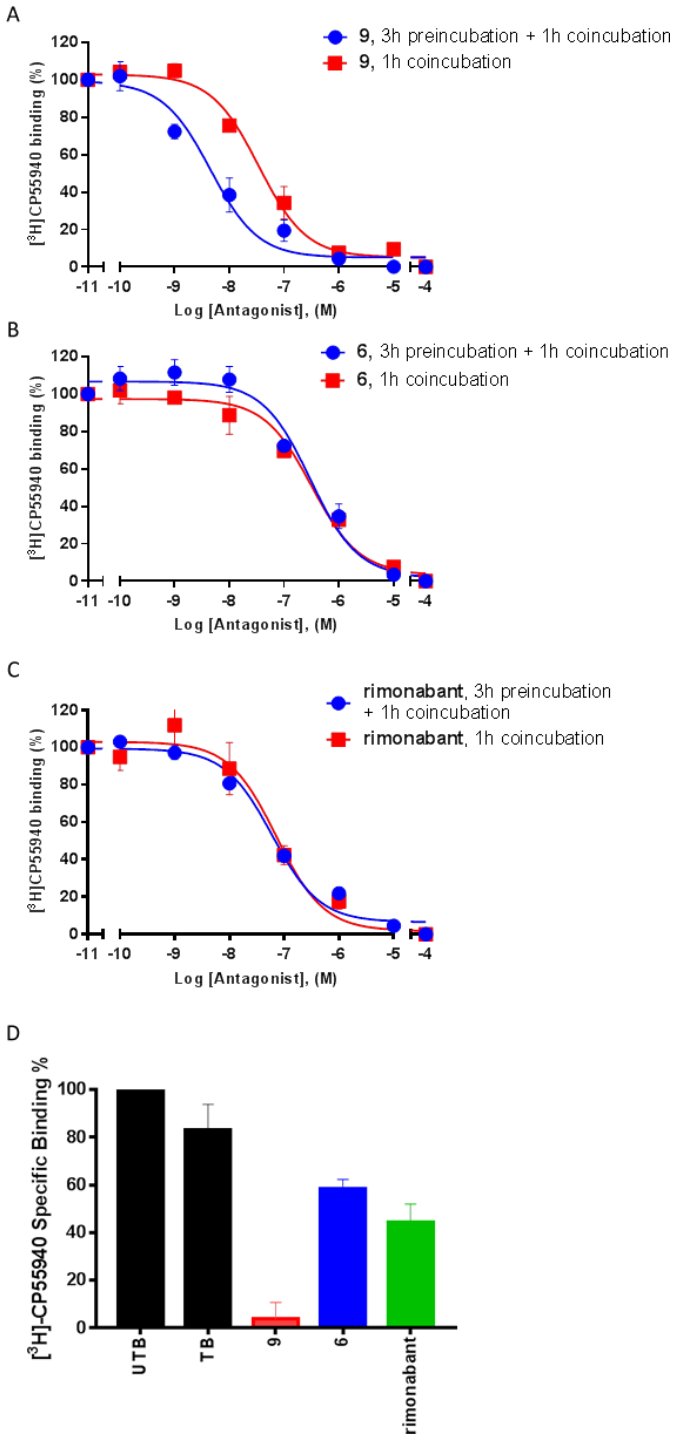

Figure 3. The "two-step incubation" experiments with [^{3}H]CP55940 binding to recombinant hCB$_1$ receptors stably expressed on CHO cell membranes (30 °C) in the absence or presence of unlabeled long-residence-time antagonist **9** (**A**), short-residence-time antagonist **6** (**B**), or reference antagonist rimonabant (**C**). Combined graphs are shown from three experiments performed in duplicate. The "wash-out" experiment with [^{3}H]CP55940 binding to recombinant hCB$_1$ receptors stably expressed on CHO cell membranes (30 °C) in the absence (UTB and TB) or presence of 1 µM of the longest RT antagonist **9** , the short RT antagonist **6** or reference antagonist rimonabant (**D**). The percentage of the specific radioligand binding relative to the unwashed blank control (UTB, 100%) is 83 ± 6.2 % for washed blank control (TB), 3.8 ± 4.1 % for antagonist **9** , 59 ± 2.2 % for antagonist **6** and 44 ± 4.4 % for rimonabant. Data are mean values ± SEM of three independent experiments in duplicate (see **Table 2** for pK$_i$ values).

The observed affinity-shift of the long RT antagonist **9** was further investigated in a "wash-out" experiment. As shown in **Figure 3D**, once the long RT antagonist **9** saturated hCB_1 receptors during pre-incubation, they could not be recovered by washing as indicated by a lack of [^{3}H]CP55940 binding, while for both short RT antagonists (**6** and rimonabant) washing of pre-saturated hCB_1 receptors did result in significant restoration of [^{3}H]CP55940 binding. Taken together, these two (pseudo-)equilibrium experiments yielded a qualitative indication that antagonist **9** had significantly slower dissociation kinetics from hCB_1 receptors than rimonabant and antagonist **6**. This was in agreement with the quantitative results obtained from the (dual-point) competition association experiments.

Computational studies on selected long and short RT antagonists.

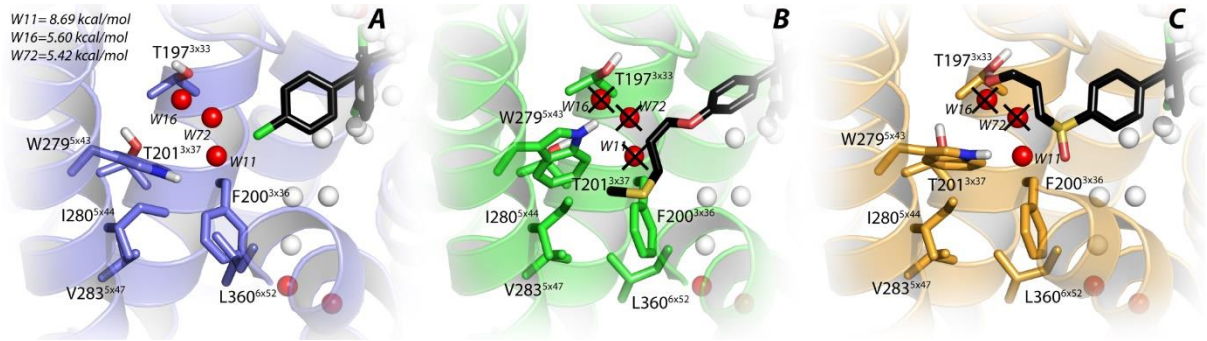

Figure 4. Docking of rimonabant (**A**), antagonist **9** (**B**) and antagonist **6** (**C**) into the binding site of the crystal structure of the hCB_1 receptor (PDB: 5TGZ)[27] co-crystalized with AM6538 (not shown), showing the overlay of numbered consecutively hydration sites of the apo-WaterMap. Hydration sites shown as red spheres represent "unstable" water molecules (>5 kcal/mol), whereas white spheres symbolize "stable" water molecules. For the unfavorable hydration centers ("unstable" water molecules) the ΔG is reported (**A**). Rimonabant is represented by black sticks, and residues within 5 Å of rimonabant are visualized as blue sticks. The protein is represented by blue ribbons (**A**). Antagonist **9** is represented by black sticks, and residues within 5 Å of **9** are visualized as green sticks. The protein is represented by green ribbons. The displaced unstable water molecule was covered with a cross (**B**). Antagonist **6** is represented by black sticks, and residues within 5 Å of **6** are visualized as yellow sticks. The displaced unstable water molecule was covered with a cross (**C**). The protein is represented by yellow ribbons. Ligand and residues atoms color code: yellow = sulfur, red = oxygen, blue = nitrogen, white = hydrogen.

In addition, to study differences between RT and binding modes, rimonabant, antagonist **6** and **9** were docked using induced-fit docking. An apo-WaterMap was generated on the basis that the small

cavity, formed by W279^{5x43}, I280^{5x44} and L360^{6x52}, could be occupied by unfavorable water molecules (W11, W16 and W72 in **Figure 4**). *W11* (ΔG = 8.69 kcal/mol) was one of the most unfavorable hydration centers in this WaterMap. This hydration center is neither displaced by rimonabant nor by the short RT antagonist **6** (**Figure 4A** and **C**). Interestingly, following from the proposed binding pose of the long RT antagonist **9**, this hydration center can be displaced by this antagonist (**Figure 4B**) as the pocket formed by the aforementioned residues is being opened.

Functional characterization of long and short RT antagonists.

Subsequently, the short RT antagonists (**6** and rimonabant) and long RT antagonist (**9**) were functionally characterized in hCB$_1$ receptor agonist-induced [^{35}S]GTPγS binding and G protein-independent (β-arrestin recruitment) assays. Firstly, their antagonistic behavior was revealed on both G protein-dependent and –independent signaling (**Table 3**), as all antagonists caused a dose-dependent decrease of agonist-induced signaling. The long RT antagonist **9** had the highest antagonistic potency in both [^{35}S]GTPγS binding and β-arrestin recruitment assays (3.0 ± 0.3 nM and 30 ± 2.7 nM, respectively), while potencies of the short RT antagonist **6** were the lowest (589 ± 96 nM and 8261 ± 179 nM, respectively). Interestingly, the antagonist potencies were significantly lower in β-arrestin recruitment compared to [^{35}S]GTPγS binding assays, where the potencies obtained from the latter were in closer agreement to the affinity values. Secondly, their mode of antagonism, i.e. surmountable or insurmountable, was investigated in both [^{35}S]GTPγS binding and β-arrestin recruitment assays. Pretreatment of CHOK1hCB1 receptor membranes ([^{35}S]GTPγS binding, **Figure 5A**) or cells (β-arrestin recruitment, **Figure 6A**) with increasing concentrations of the long RT antagonist **9** before stimulation by the CB$_1$ receptor agonist CP55940 induced insurmountable antagonism (**Figure 5A**). In other words, the CP55940 concentration-effect curves were shifted to the right with a concomitant decrease in the maximal response. Conversely, the short RT antagonists (**6** and rimonabant) displayed surmountable antagonism, i.e. shifting CP55940's curves to the right

without affecting its maximum effect ([^{35}S]GTPγS binding, **Figure 5C, E;** and β-arrestin recruitment, **Figure 6C, E**).

Table 3. Functional effects of selected long (**9**) and short (**6**) RT hCB$_1$ receptor antagonists determined by [^{35}S]GTPγS binding and β-arrestin recruitment assays, using rimonabant as a reference.

n ≥ 3		**Antagonist potency**	**Antagonist (in)surmountability**				**Inverse agonism**
			Preincubation		Coincubation		
	Antagonist	pIC$_{50}$ ± SEM (IC$_{50}$ in nM) [a]	*p*A$_2$ [b]	Schild slope [b]	*p*A$_2$ [b]	Schild slope [b]	pIC$_{50}$ ± SEM (IC$_{50}$ in nM) [c]
[^{35}S]GTPγS binding assays	**9**	8.5 ± 0.0 (3.0)	N.A.[d]	N.A.	8.9 ± 0.0	2.4 ± 0.2	8.6 ± 0.1 (2.7)
	6	6.3 ± 0.1 (589)	8.5 ± 0.5	1.0 ± 0.2	9.1 ± 0.2	1.1 ± 0.0	7.1 ± 0.1 (84)
	Rimonabant	8.0 ± 0.1 (11)	10 ± 0.2	1.3 ± 0.1	10 ± 0.3	1.2 ± 0.2	8.4 ± 0.1 (4.0)
β-arrestin recruitment assays	**9**	7.5 ± 0.0 (30)	N.A.	N.A.	8.1 ± 0.1	1.8 ± 0.0	6.8 ± 0.2 (165)
	6	5.1 ± 0.0 (8261)	6.4 ± 0.0	1.2 ± 0.2	7.7 ± 0.1	0.7 ± 0.2	6.8 ± 0.2 (179)
	Rimonabant	6.8 ± 0.1 (184)	8.0 ± 0.2	1.3 ± 0.3	8.2 ± 0.4	1.2 ± 0.3	6.3 ± 0.2 (627)

[a] pIC$_{50}$ ± SEM, obtained from either [^{35}S]GTPγS binding (n = 4) or β-arrestin recruitment (n = 3) assays on recombinant human CB$_1$ receptors stably expressed on CHO cell membranes or intact cell line.

[b] Obtained from Schild analyses, [^{35}S]GTPγS binding assays (n = 3) or β-arrestin recruitment assays (n=3, except for pre-incubation assays with Rimonabant n = 5).

[c] pIC$_{50}$ ± SEM, obtained from either [^{35}S]GTPγS binding (n = 3) or β-arrestin recruitment (n = 3) assays on recombinant human CB$_1$ receptors stably expressed on CHO cell membranes or intact cell line.

[d] N.A. not applicable.

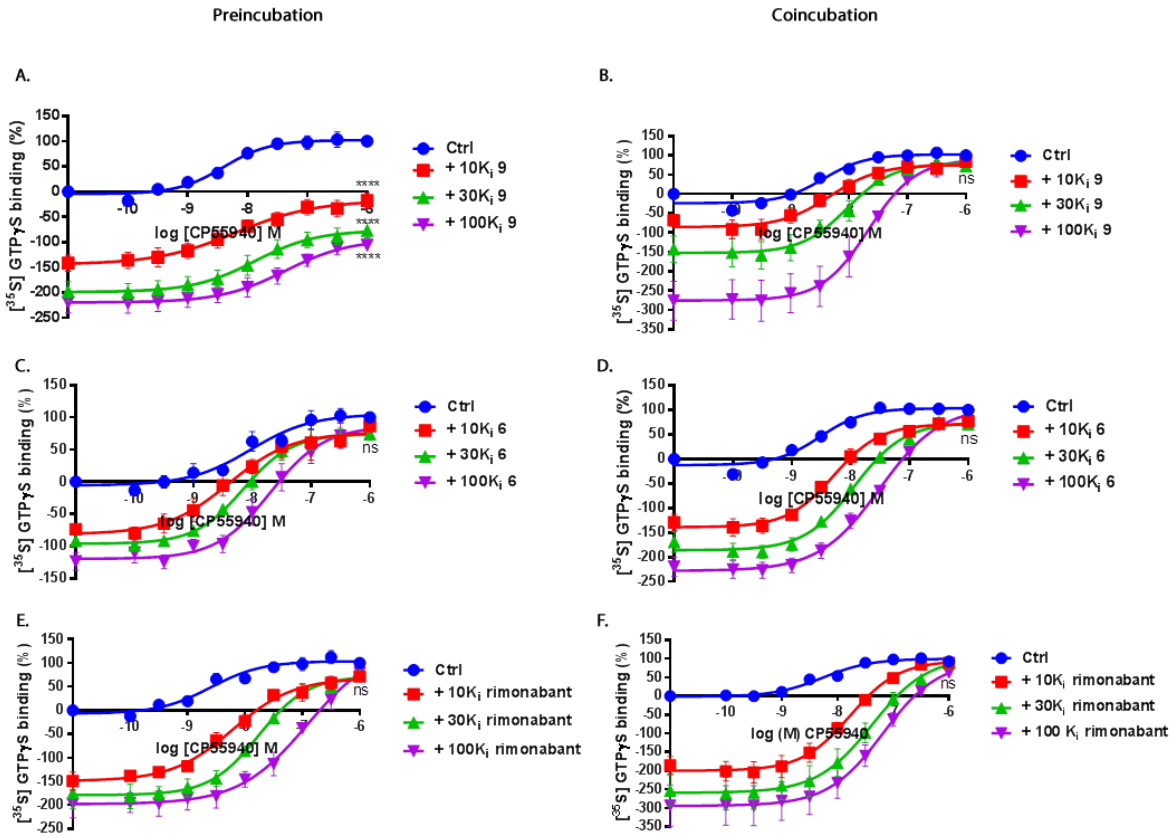

Figure 5. CP55940-stimulated [^{35}S]GTPγS binding to recombinant hCB$_1$ receptors stably expressed on CHO cell membranes (30 °C) in the absence or presence of long-residence-time antagonist **9** (**A** and **B)**, short-residence-time antagonist **6** (**C** and **D)** and reference antagonist rimonabant (**E** and **F**). Antagonist **9** (**A**), **6** (**C**) or rimonabant (**E**) were either incubated for 60 min prior to the challenge with the hCB$_1$ receptor agonist CP55940 or coincubated with CP55940 (antagonist **9, B**, antagonist **6, D** or rimonabant, **F**). The agonist curves were generated in the presence of increasing concentrations of antagonist, namely 10-, 30-, 100-fold their respective K_i values. The shift in agonist EC_{50} was determined to perform Schild analyses. Two-way ANOVA with Tukey's post-test was applied for the comparison of E_{max} by agonist control, **** $p < 0.0001$, ns for not significant. Data were normalized according to the maximal response (100%) produced by CP55940. Combined graphs are shown from three experiments performed in duplicate (see **Table 3** for pA_2 and Schild-slope values).

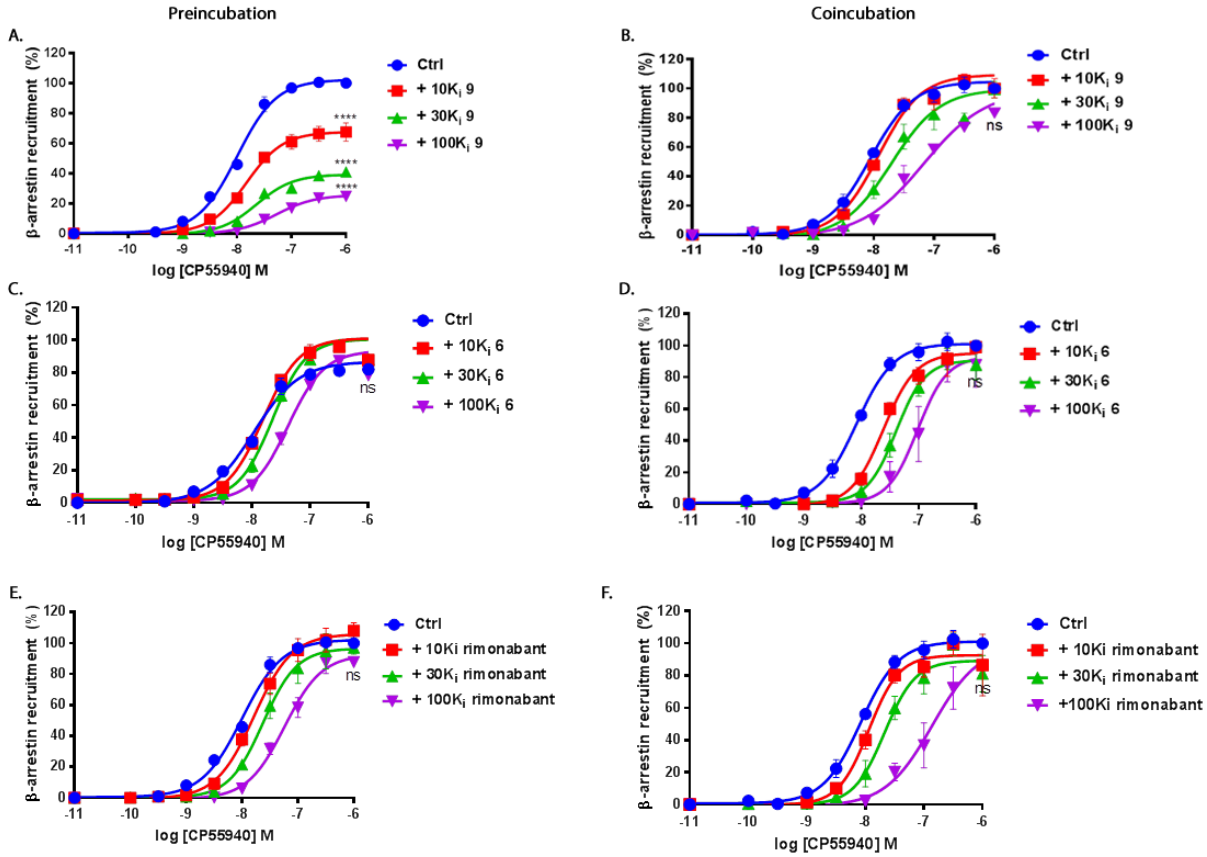

Figure 6. CP55940-stimulated β-arrestin recruitment to recombinant hCB_1 receptors stably expressed on CHO cells (37 °C and 5 % CO_2) in the absence or presence of long-residence-time antagonist **9** (**A** and **B**), short-residence-time antagonist **6** (**C** and **D**) and reference antagonist rimonabant (**E** and **F**). Antagonist **9** (**A**), **6** (**C**) or rimonabant (**E**) were either incubated for 60 min prior to the challenge of the hCB_1 receptor agonist CP55940 or were coincubated with CP55940 (antagonist **9, B**, antagonist **6, D** or rimonabant, **F**). The agonist curves were generated in the presence of increasing concentrations of antagonist, namely 10-, 30-, 100-fold their respective K_i values. The shift in agonist EC_{50} was determined to perform Schild analyses. Two-way ANOVA with Tukey's post-test was applied for the comparison of E_{max} by agonist control, **** $p < 0.0001$, ns for not significant. Data were normalized according to the maximal response (100%) produced by CP55940. Combined graphs are shown from at least three experiments performed in duplicate (n=3, except for pre-incubation assays with Rimonabant n=5). See **Table 3** for pA_2 and Schild-slope values.

Under such experimental set-up, the obtained Schild-slopes of both **6** and rimonabant were close to unity in either [^{35}S]GTPγS binding or β-arrestin recruitment assays (**Table 3**). Moreover, from [^{35}S]GTPγS binding assays the pA_2 value of **6** was close to its pK_i value (8.5 ± 0.5 from Table **3** vs 7.9 ±

0.01 from **Table 2**), while for rimonabant these were more divergent (10 ± 0.2 from **Table 3** vs 8.8 ± 0.1 from **Table 2**). In addition, pA_2 values derived from β-arrestin recruitment assays for **6** and rimonabant were less comparable with the corresponding pK_i values. Next, we performed co-incubation experiments with these antagonists in the presence of CP55940 ([^{35}S]GTPγS binding, **Figure 5B, D, F**; and β-arrestin recruitment, **Figure 6B, D, F**). In this experimental set-up, all antagonists produced a rightward shift in the CP55940 concentration-effect curves without a suppression of the maximal response. Notably, the Schild-slopes of the short RT antagonists (**6** and rimonabant) were close to unity in both [^{35}S]GTPγS binding (1.1 ± 0.0 for **6**, 1.2 ± 0.2 for rimonabant, **Table 3**) and β-arrestin recruitment assays (0.7 ± 0.2 for **6**, 1.2 ± 0.3 for rimonabant, **Table 3**). In contrast, for the long RT antagonist **9** the Schild-slope derived from both assays was well above unity (**Table 3**).

Inverse agonism of the selected CB_1 antagonists.

Finally, it became clear from the [^{35}S]GTPγS binding assays that the antagonists behaved as inverse agonists (**Figure 7A**). It follows that all antagonists caused a dose-dependent decrease of basal [^{35}S]GTPγS binding. The short RT antagonist **6** was 21-fold less potent as an inverse agonist than short RT rimonabant, while the latter was actually equally potent to the long RT antagonist **9** (**Table 3).** Furthermore, we decided to investigate the presence of inverse agonism in the β-arrestin recruitment assay. After adjusting the standard protocol (i.e. extending the incubation time from 90 min to 6 h) inverse agonism was observed for all antagonists (**Figure 7B** and **Table 3**), as in the [^{35}S]GTPγS binding assays. Rimonabant was the least potent inverse agonist in the β-arrestin recruitment assay (IC_{50} = 627 nM), while the short RT and long RT antagonist had a similar potency (**6:** IC_{50} = 179 nM and **9:** IC_{50} = 165 nM, respectively). Overall, the inverse agonistic potencies in β-arrestin recruitment assays were significantly lower than those obtained in the [^{35}S]GTPγS binding assays.

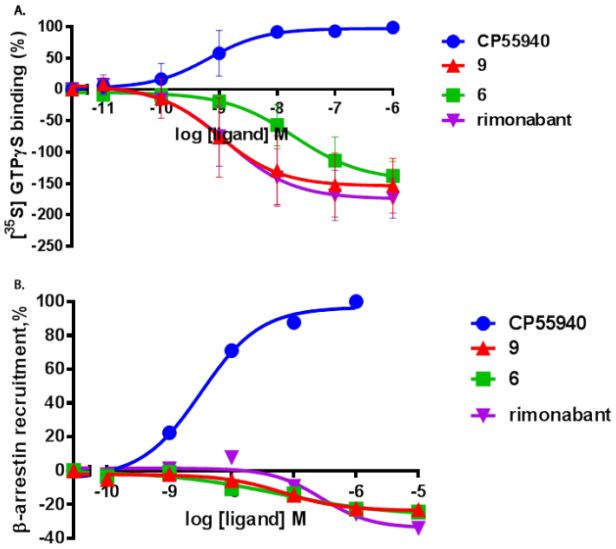

Figure 7. Characterization of inverse agonism for long RT antagonist **9**, short RT antagonist **6** and reference antagonist rimonabant. [^{35}S]GTPγS binding to recombinant hCB_1 receptors stably expressed on CHO cell membranes (**A**) or β-arrestin recruitment to recombinant hCB_1 receptors stably expressed on CHO cells (**B**) with ligand concentrations ranging from 0.1 nM to 10 µM. Data were normalized according to the maximal response (100%) produced by CP55940. Combined graphs are shown from three experiments performed in duplicate in **A**; a representative graph is shown from one experiment performed in duplicate in **B** (see **Table 3** for pIC_{50} values).

Discussion

Ligand optimization based on Structure–Kinetics Relationships (SKR).

Receptor binding kinetics is increasingly being recognized as an important parameter to understand a drug's mechanism of action and ultimately improve its *in vivo* efficacy and safety. Here we focused on the substitutions at the thiophene's 3-position (R group) in a series of rimonabant related antagonists (**Table 1**). Applying equilibrium and kinetic radioligand binding assays, we assayed the binding interactions of nine of such hCB_1 receptor antagonists together with the reference compound rimonabant. As a result, diverse affinity and KRI values were determined and both long and short RT antagonists were identified. Interestingly, the recent hCB_1 receptor crystal structures indicate that the aliphatic R-substitutions fit in the lipophilic "long and narrow channel" of the hCB_1 receptor.[27, 39] Apparently, targeting this channel with diversified chemical fragments is highly relevant

for the improvement of binding interactions at the hCB_1 receptor. Specifically from antagonists **6** (RT = 19 min) and **9** (RT = 2222 min) it seems that a longer (6- vs 5-atom) tail with less polarity contributes significantly to slow receptor dissociation kinetics and better affinity (1.4 nM of **9** vs 14 nM of **6**).Interestingly, the more than 100-fold gain in residence time is not fully reflected in the increase in affinity. This may in part be due to the entropic cost of the aliphatic chain when it has to adapt to the steric requirements of the hydrophobic channel of the binding site, resulting in a slower association rate.[40] Taken together, this limited SKR study proves that kinetic profiles should and can be taken into account during the lead optimization process in drug discovery.

The computational insights of the binding modes.

Using the crystal structure of the hCB_1-AM6538 complex (PDB: 5TGZ),[27] we performed WaterMap calculations to try and understand the differences in residence times observed for the hCB_1 receptor antagonists studied, with the hypothesis that unfavorable hydration might provide an explanation.[34, 35, 41, 42] We focused on antagonist **9** and **6**, and in particular the substitutions at the thiophene's 3-position (R-group) as this was the only structural difference (**Figure 4**). When the antagonist with the shorter and more hydrophilic side chain (**6**, $-SO_2CH_2CH_2CH_2OH$, short RT) was docked into the apo WaterMap, it was able to displace water molecules found in positions *W16* and *W72;* while unstable water molecule *W11* was still around its side chain (**Figure 4C**). We propose that the interaction with $T197^{3x33}$ forces **6** in an orientation where its sulfonyl further stabilized water molecules found in position *W11*. By contrast, antagonist **9** was able to displace all these water molecules (*W11*, *W16* and *W72*) with its longer and more hydrophobic side chain, a process which might raise the energy of the transition state for dissociation (**Figure 4B**). We postulate that this destabilization of the transition state may contribute to the prolonged RT observed with this compound. In contrast, rimonabant cannot displace those unhappy water similarly to antagonist **6**, due to its lack of the linear side chain reaching those energetically unfavorable or unhappy waters (**Figure 4A**).

Methodological aspects on radioligand binding assays.

A so-called dual-point competition association assay for hCB_1 receptor was applied for the "kinetic screening campaign" to increase throughput in comparison to the traditional competition association experiments as shown before.[30] A good correlation between the antagonists' KRI values and dissociation rate constants (k_{off}, k_4) corroborated the robustness of this assay (**Figure 2A**). In contrast, no significant correlations were found between the kinetic binding parameters, k_{on} (k_3) or k_{off} (k_4), and affinity values of these antagonists (**Figure 2 C, D**). Besides, the equilibrium K_i and kinetic K_D values were significantly correlated (**Figure 2B**). Noteworthy, the extraordinary long RT antagonist **9** (**Figure 3,** highlighted in red color) was observed as a significant "outlier" in the correlation plots involving the affinity values obtained from equilibrium assays (**Figure 2B, D**). This clearly indicates that equilibrium was not reached for this antagonist during the radioligand displacement assay where a relatively short incubation time is used. In general, equilibrium affinities of long RT antagonists might often be underestimated and this potentially results in ignoring such interesting compounds for further evaluation.

Subsequently, we designed a "two-step incubation" experiment for further investigation of the affinity-shift of short and long RT antagonists. The displacement curve of the long RT antagonists **9** was shifted leftward about 10-fold, compared to a standard affinity determination, which was then similar to its calculated kinetic K_D (**Table 1** and **2**). In contrast, the affinity of short RT antagonists (**6** and rimonabant) determined in the "two-step incubation" and standard experiments showed no such shift (**Table 2**). These results once more indicate that during a longer period of incubation in the absence of a competing ligand a larger fraction of antagonist **9** forms a tight and slowly dissociating ligand-receptor complex. During preincubation the antagonist **9** enjoys a binding "monopoly" to hCB_1 receptors and the occupied hCB_1 receptors are pseudo-irreversibly blocked, as antagonist **9** (with its extremely long RT) is unlikely to dissociate again. Such a potential two-step (or multi-step) bimolecular binding has also been reported for CCR5 antagonists, where a shift in the apparent affinity was also reported after pre-incubation.[43] Moreover, the pseudo-irreversible binding of long RT antagonist **9** was also confirmed in "wash-out" experiments, where its binding to hCB_1 receptors

was washing-resistant, while short RT antagonists **6** and rimonabant were washed away more easily (**Figure 3D**). A washing-resistant effect has been reported more often for covalently binding ligands to various targets.[44-46] While the current study was mostly focused on developing methodologies for investigating whether the addition of SKR would result in a different triaging of CB_1 antagonists, we are aware that the translation to native tissues should be made. For example, it is known that CB_1 receptors are the most highly expressed receptors in the brain, where they have been shown to form functional heteromers with other GPCR, such as adenosine A_{2A} receptors[47] and beta2 adrenergic receptors.[48] Although this has yet to be investigated for CB_1 receptors, a ligand's binding kinetics is likely to be very different on a monomer than a (hetero)dimer as was recently shown for homodimers of adenosine A_3 receptors.[49, 50]

The functional effects of long or short RT human CB_1 receptor antagonists.

Diverging dissociation rate constants of antagonists have been linked to differentiation in functional effects (i.e. surmountable vs insurmountable antagonism) and concomitant physiological relevance, even before the concept of kinetic studies was gaining acceptance.[51, 52] In our studies, the differences in binding interactions between long and short RT antagonists (**9** vs **6** and rimonabant) prompted us to further investigate potential differences in functional effects. In both [^{35}S]GTPγS binding and β-arrestin recruitment assays, long RT antagonist **9** generated an insurmountable effect when preincubated before stimulation with the agonist CP55940 (**Figure 5A** and **6A**). Importantly, when the preincubation was excluded, its effects became surmountable proving that (**Figure 5B** and **6B**) the long RT antagonist **9** prevents the agonist CP55940 to activate receptors by competitive pseudo-irreversible binding to hCB_1 receptors, as opposed to allosterically inhibiting CP55940 activation.[53, 54] Since the short RT antagonists (**6** and rimonabant) do not occupy hCB_1 receptors for that long, CP55940 was able to activate hCB_1 receptors in the presence of such antagonists under all experimental conditions, which resulted in surmountable antagonism (**Figure 5C-F** and **6C-F**). Moreover, the surmountable effect can be quantified through competitive Gaddum-Schild analysis.[55]

Here for the short RT antagonists (**6** and rimonabant) Schild-slopes close-to-unity were obtained, which indicated a one-to-one competition with the agonist CP55940 while equilibrium was reached. Interestingly, the Schild-slopes determined in the coincubation experiments of long RT antagonist **9** were above 1, i.e. the EC_{50} shifts were greater than predicted by such analysis. This effect can again be explained by its pseudo-irreversible binding to the hCB_1 receptor, where equilibrium was not reached at the chosen incubation times. Of note, in native systems (i.e. under non-equilibrium conditions) endocannabinoid exposure is high, but short due to metabolic degradation of the agonist.[56, 57] However, long and short RT antagonists will still differentiate under these circumstances, as an insurmountable antagonist (i.e. with long RT) can cope with the high local concentrations of the endogenous agonist , while the short RT antagonist cannot. One last note is on the applicability domain of a Schild-plot analysis. Strictly speaking this analysis was derived for systems without constitutive activity, while its use for other systems, i.e. displaying constitutive activity like in our study, has been (re)considered.[58] From Kenakin's reasoning it appears that a small overestimation of the potency of inverse agonists is possible.

Secondly, the selected long or short RT hCB_1 receptor antagonists (**9**, **6** and rimonabant[59]) behaved as inverse agonists in the standard [^{35}S]GTPγS binding assays (**Table 3, Figure 7A**). In the β-arrestin recruitment assay inverse agonism was only observed when the assay-kit manufacturer's protocol was adjusted to contain a longer incubation time (i.e. 6-hour instead of 90 min) (**Figure 7B**).[31] Of note, the cells tolerated this increased incubation time, since the potency of the reference agonist CP55940 did not change (data not shown). The inverse agonism at cannabinoid receptors (i.e. CB_1 and CB_2) in the β-arrestin recruitment assay has been seldom reported.[60] Importantly, although we have used a cell line that heterologously (and abundantly) expresses CB_1 receptors which might raise the question that the level of constitutive activity is an artefact, it is known that this receptor is the highest expressed GPCR in the brain.[61, 62] Moreover, the scientific community, including pharmaceutical industry, actually prompted that the inverse agonistic characteristic might be the

cause of adverse side effects seen with CB_1 antagonists and is therefore in pursuit of 'neutral' antagonists.[63, 64] Noteworthy, there was no correlation between inverse agonism and RTs.

Lastly, the CB_1 receptor is a class A GPCR and it has been reported that its down-stream signaling pathways involve both G protein-coupling and β-arrestin recruitment.[65] When comparing the functional results from [^{35}S]GTPγS binding and β-arrestin recruitment, we learned the antagonists were more potent in the former. Recently, it was reported that hCB_1 receptor activation can trigger 3 "waves" of signaling, G protein-coupling as the first, β-arrestin recruitment as the second, and a combination of the two as the last.[66] The possible correlation between binding kinetics and signaling effects on the CB_1 receptor merits further investigation.

In conclusion, we have evaluated the binding kinetics of nine 1-(4,5-diarylthiophene-2-carbonyl)-4-phenylpiperidine-4-carboxamide derivatives at the hCB_1 receptor, and described structure-kinetics relationships (SKR) defined by their Kinetic Rate Index (KRI) values and dissociation rate constants. The antagonist **9** was found to be a pseudo-irreversible hCB_1 receptor antagonist with a residence time of 2222 min at 30 ^{o}C. Moreover, the difference in receptor-ligand interaction (i.e. long vs short RT) was correlated with the mode of functional antagonism (insurmountable vs surmountable), as determined for both G protein-dependent and –independent signaling pathways. Following from docking studies and WaterMap calculations, we speculate that displacement of unfavorable water molecules may provide a plausible explanation for antagonist **9**'s slow dissociation, or even pseudo-irreversible binding at the hCB_1 receptor. These findings could be highly valuable for the further development of potent and safe CB_1 receptor antagonists for metabolic disorders such as obesity.

References

1. Maccarrone, M.; Bab, I.; Bíró, T.; Cabral, G. A.; Dey, S. K.; Di Marzo, V.; Konje, J. C.; Kunos, G.; Mechoulam, R.; Pacher, P.; Sharkey, K. A.; Zimmer, A. Endocannabinoid signaling at the periphery: 50 years after THC. *Trends Pharmacol. Sci.* **2015,** *36*, 277-296.

2. Pertwee, R. G.; Howlett, A. C.; Abood, M. E.; Alexander, S. P. H.; Di Marzo, V.; Elphick, M. R.; Greasley, P. J.; Hansen, H. S.; Kunos, G.; Mackie, K.; Mechoulam, R.; Ross, R. A. International union of basic and clinical pharmacology. LXXIX. cannabinoid receptors and their ligands: beyond CB_1 and CB_2. *Pharmacol. Rev.* **2010,** *62*, 588-631.
3. Howlett, A. C. Cannabinoid inhibition of adenylate cyclase. Biochemistry of the response in neuroblastoma cell membranes. *Mol. Pharmacol.* **1985,** 27, 429-436.
4. Jin, W.; Brown, S.; Roche, J. P.; Hsieh, C.; Celver, J. P.; Kovoor, A.; Chavkin, C.; Mackie, K. Distinct domains of the CB_1 cannabinoid receptor mediate desensitization and internalization. *J. Neurosci.* **1999,** 19, 3773-3780.
5. Abood, M.; Barth, F.; Bonner, T. I.; Cabral, G.; Casellas, P.; Cravatt, B. F.; Devane, W. A.; Elphick, M. R.; Felder, C. C.; Herkenham, M.; Howlett, A. C.; Kunos, G.; Mackie, K.; Martin, B. R.; Mechoulam, R.; Pertwee, R. G. Cannabinoid receptors: CB_1 receptor. http://www.guidetopharmacology.org/GRAC/ObjectDisplayForward?objectId=56. (December 8).
6. Pacher, P.; BÁTkai, S.; Kunos, G. The endocannabinoid system as an emerging target of pharmacotherapy. *Pharmacol. Rev.* **2006,** *58*, 389-462.
7. Bermudez-Silva, F. J.; Viveros, M. P.; McPartland, J. M.; Rodriguez de Fonseca, F. The endocannabinoid system, eating behavior and energy homeostasis: the end or a new beginning? *Pharmacol., Biochem. Behav.* **2010,** *95*, 375-382.
8. Perkins, J. M.; Davis, S. N. Endocannabinoid system overactivity and the metabolic syndrome: prospects for treatment. *Curr. Diabetes Rep.* **2008,** *8*, 12-19.
9. Lu, D.; Dopart, R.; Kendall, D. A. Controlled downregulation of the cannabinoid CB_1 receptor provides a promising approach for the treatment of obesity and obesity-derived type 2 diabetes. *Cell Stress Chaperones* **2016,** 21, 1-7.
10. FDA briefing document NDA 21-888 zimulti (rimonabant) tablets, 20 mg sanofi aventis advisory committee. Published on June 13, 2007. Accessed on July 20, 2017. <http://www.fda.gov/ohrms/dockets/ac/07/briefing/2007-4306b1-fda-backgrounder.pdf>.
11. Topol, E. J.; Bousser, M.-G.; Fox, K. A. A.; Creager, M. A.; Despres, J.-P.; Easton, J. D.; Hamm, C. W.; Montalescot, G.; Steg, P. G.; Pearson, T. A.; Cohen, E.; Gaudin, C.; Job, B.; Murphy, J. H.; Bhatt, D. L. Rimonabant for prevention of cardiovascular events (CRESCENDO): a randomised, multicentre, placebo-controlled trial. *Lancet* **2010,** *376*, 517-523.
12. Boekholdt, S. M.; Peters, R. J. G. Rimonabant: obituary for a wonder drug. *Lancet* **2010,** *376*, 489-490.
13. Mitchell, P. B.; Morris, M. J. Depression and anxiety with rimonabant. *Lancet* **2007,** 370, 1671-1672.
14. Röver, S.; Andjelkovic, M.; Bénardeau, A.; Chaput, E.; Guba, W.; Hebeisen, P.; Mohr, S.; Nettekoven, M.; Obst, U.; Richter, W. F.; Ullmer, C.; Waldmeier, P.; Wright, M. B. 6-Alkoxy-5-aryl-3-pyridinecarboxamides, a new series of bioavailable cannabinoid receptor type 1 (CB_1) antagonists including peripherally selective compounds. *J. Med. Chem.* **2013,** 56, 9874-9896.
15. Abdel-Magid, A. F. Treatment of metabolic disorders with CB_1 receptor inverse agonists. *ACS Med. Chem. Lett.* **2016,** 7, 874-875.
16. Klumpers, L. E.; Fridberg, M.; de Kam, M. L.; Little, P. B.; Jensen, N. O.; Kleinloog, H. D.; Elling, C. E.; van Gerven, J. M. A. Peripheral selectivity of the novel cannabinoid receptor antagonist TM38837 in healthy subjects. *Br. J. Clin. Pharmacol.* **2013,** 76, 846-857.
17. Dow, R. L.; Carpino, P. A.; Gautreau, D.; Hadcock, J. R.; Iredale, P. A.; Kelly-Sullivan, D.; Lizano, J. S.; O'Connor, R. E.; Schneider, S. R.; Scott, D. O.; Ward, K. M. Design of a potent CB_1 receptor antagonist series: potential scaffold for peripherally-targeted agents. *ACS Med. Chem. Lett.* **2012,** 3, 397-401.
18. Guo, D.; Hillger, J. M.; IJzerman, A. P.; Heitman, L. H. Drug-target residence time—A case for G protein-coupled receptors. *Med. Res. Rev.* **2014,** 34, 856-892.
19. Swinney, D. C.; Haubrich, B. A.; van Liefde, I.; Vauquelin, G. The role of binding kinetics in GPCR drug discovery. *Curr. Top. Med. Chem.* **2015,** *15*, 2504-2522.

20. Copeland, R. A. The drug-target residence time model: a 10-year retrospective. *Nat. Rev. Drug Discovery* **2016,** *15*, 87-95.
21. Vilums, M.; Zweemer, A. J. M.; Yu, Z.; de Vries, H.; Hillger, J. M.; Wapenaar, H.; Bollen, I. A. E.; Barmare, F.; Gross, R.; Clemens, J.; Krenitsky, P.; Brussee, J.; Stamos, D.; Saunders, J.; Heitman, L. H.; IJzerman, A. P. Structure–kinetic relationships—an overlooked parameter in hit-to-lead optimization: a case of cyclopentylamines as chemokine receptor 2 antagonists. *J. Med. Chem.* **2013,** *56*, 7706-7714.
22. Guo, D.; Xia, L.; van Veldhoven, J. P. D.; Hazeu, M.; Mocking, T.; Brussee, J.; IJzerman, A. P.; Heitman, L. H. Binding kinetics of ZM241385 derivatives at the human adenosine A_{2A} receptor. *ChemMedChem* **2014,** *9*, 752-761.
23. Louvel, J.; Guo, D.; Agliardi, M.; Mocking, T. A. M.; Kars, R.; Pham, T. P.; Xia, L.; de Vries, H.; Brussee, J.; Heitman, L. H.; IJzerman, A. P. Agonists for the adenosine A_1 receptor with tunable residence time. A case for nonribose 4-amino-6-aryl-5-cyano-2-thiopyrimidines. *J. Med. Chem.* **2014,** *57*, 3213-3222.
24. Xia, L.; Burger, W. A. C.; van Veldhoven, J. P. D.; Kuiper, B. J.; van Duijl, T. T.; Lenselink, E. B.; Paasman, E.; Heitman, L. H.; IJzerman, A. P. Structure–affinity relationships and structure–kinetics relationships of pyrido[2,1-f]purine-2,4-dione derivatives as human adenosine A_3 receptor antagonists. *J. Med. Chem.* **2017,** *60*, 7555-7568.
25. Barth, F.; Ducoux, J. P.; Gueule, P.; Rinaldi-Carmona, M.; Rouquette, A. Thiophene-2-carboxamide derivatives, preparation thereof and therapeutic use thereof (2010) Patent Application WO2010012964. In 2010.
26. Ducoux, J. P.; Rinaldi-Carmona, M.; Rouquette, A. Derives de 3-alcoxy-4,5-diarylthiophene-2-carboxamide, leur preparation et leur application en therapeutique (2010) Patent Application WO2010109150. In 2010.
27. Hua, T.; Vemuri, K.; Pu, M.; Qu, L.; Han, Gye W.; Wu, Y.; Zhao, S.; Shui, W.; Li, S.; Korde, A.; Laprairie, Robert B.; Stahl, Edward L.; Ho, J.-H.; Zvonok, N.; Zhou, H.; Kufareva, I.; Wu, B.; Zhao, Q.; Hanson, Michael A.; Bohn, Laura M.; Makriyannis, A.; Stevens, Raymond C.; Liu, Z.-J. Crystal Structure of the Human Cannabinoid Receptor CB_1. *Cell* **2016,** 167, 750-762.e714.
28. Xia, L.; Vries, H.; IJzerman, A. P.; Heitman, L. H. Scintillation proximity assay (SPA) as a new approach to determine a ligand's kinetic profile. A case in point for the adenosine A1 receptor. *Purinergic Signalling* **2015,** 12, 115-126.
29. Motulsky, H. J.; Mahan, L. C. The kinetics of competitive radioligand binding predicted by the law of mass action. *Molecular Pharmacology* **1984,** 25, 1-9.
30. Guo, D.; van Dorp, E. J. H.; Mulder-Krieger, T.; van Veldhoven, J. P. D.; Brussee, J.; IJzerman, A. P.; Heitman, L. H. Dual-point competition association assay: a fast and high-throughput kinetic screening method for assessing ligand-receptor binding kinetics. *J. Biomol. Screening* **2013,** 18, 309-320.
31. https://www.discoverx.com/DiscoveRx/media/ContentFiles/DataSheets/93-0001M.pdf.
32. Schrödinger Release 2017-2: Schrödinger Suite 2017-2 Protein Preparation Wizard; Epik, Schrödinger, LLC, New York, NY, 2017; Impact, Schrödinger, LLC, New York, NY, 2017; Prime, Schrödinger, LLC, New York, NY, 2017.
33. Sherman, W.; Day, T.; Jacobson, M. P.; Friesner, R. A.; Farid, R. Novel procedure for modeling ligand/receptor induced fit effects. *J. Med. Chem.* **2006,** *49*, 534-553.
34. Abel, R.; Young, T.; Farid, R.; Berne, B. J.; Friesner, R. A. Role of the active-site solvent in the thermodynamics of Factor Xa ligand binding. *J. Am. Chem. Soc.* **2008,** *130*, 2817-2831.
35. Young, T.; Abel, R.; Kim, B.; Berne, B. J.; Friesner, R. A. Motifs for molecular recognition exploiting hydrophobic enclosure in protein–ligand binding. *Proc. Natl. Acad. Sci. U. S. A.* **2007,** *104*, 808-813.
36. Schrödinger, L. L. C., New York. *The PyMOL molecular graphics system*, 1.8.3.2; **2016**.
37. Cheng, Y.-C.; Prusoff, W. H. Relationship between the inhibition constant (K_i) and the concentration of inhibitor which causes 50 percent inhibition (IC_{50}) of an enzymatic reaction. *Biochem. Pharmacol.* **1973,** 22, 3099-3108.

38. Soethoudt, M.; Grether, U.; Fingerle, J.; Grim, T. W.; Fezza, F.; de Petrocellis, L.; Ullmer, C.; Rothenhäusler, B.; Perret, C.; van Gils, N.; Finlay, D.; MacDonald, C.; Chicca, A.; Gens, M. D.; Stuart, J.; de Vries, H.; Mastrangelo, N.; Xia, L.; Alachouzos, G.; Baggelaar, M. P.; Martella, A.; Mock, E. D.; Deng, H.; Heitman, L. H.; Connor, M.; Di Marzo, V.; Gertsch, J.; Lichtman, A. H.; Maccarrone, M.; Pacher, P.; Glass, M.; van der Stelt, M. Cannabinoid CB_2 receptor ligand profiling reveals biased signalling and off-target activity. *Nat. Commun.* **2017,** 8, 13958-13972.
39. Shao, Z.; Yin, J.; Chapman, K.; Grzemska, M.; Clark, L.; Wang, J.; Rosenbaum, D. M. High-resolution crystal structure of the human CB_1 cannabinoid receptor. *Nature* **2016,** 540, 602-606.
40. Weiß, R. G.; Setny, P.; Dzubiella, J. Principles for tuning hydrophobic ligand–receptor binding kinetics. *J. Chem. Theory Comput.* **2017,** 10.1021/acs.jctc.1027b00216.
41. Segala, E.; Guo, D.; Cheng, R. K. Y.; Bortolato, A.; Deflorian, F.; Doré, A. S.; Errey, J. C.; Heitman, L. H.; IJzerman, A. P.; Marshall, F. H.; Cooke, R. M. Controlling the dissociation of ligands from the adenosine A_{2A} receptor through modulation of salt bridge strength. *J. Med. Chem.* **2016,** *59*, 6470-6479.
42. Pearlstein, R. A.; Sherman, W.; Abel, R. Contributions of water transfer energy to protein-ligand association and dissociation barriers: Watermap analysis of a series of p38α MAP kinase inhibitors. *Proteins: Struct., Funct., Bioinf.* **2013,** 81, 1509-1526.
43. Swinney, D. C.; Beavis, P.; Chuang, K.-T.; Zheng, Y.; Lee, I.; Gee, P.; Deval, J.; Rotstein, D. M.; Dioszegi, M.; Ravendran, P.; Zhang, J.; Sankuratri, S.; Kondru, R.; Vauquelin, G. A study of the molecular mechanism of binding kinetics and long residence times of human CCR5 receptor small molecule allosteric ligands. *Br. J. Pharmacol.* **2014,** 171, 3364-3375.
44. Yang, X.; Dong, G.; Michiels, T. J. M.; Lenselink, E. B.; Heitman, L.; Louvel, J.; IJzerman, A. P. A covalent antagonist for the human adenosine A_{2A} receptor. *Purinergic Signalling* **2016,** 13, 191-201.
45. Tan, L.; Wang, J.; Tanizaki, J.; Huang, Z.; Aref, A. R.; Rusan, M.; Zhu, S.-J.; Zhang, Y.; Ercan, D.; Liao, R. G.; Capelletti, M.; Zhou, W.; Hur, W.; Kim, N.; Sim, T.; Gaudet, S.; Barbie, D. A.; Yeh, J.-R. J.; Yun, C.-H.; Hammerman, P. S.; Mohammadi, M.; Jänne, P. A.; Gray, N. S. Development of covalent inhibitors that can overcome resistance to first-generation FGFR kinase inhibitors. *Proc. Natl. Acad. Sci. U. S. A.* **2014,** 111, E4869-E4877.
46. Leonti, M.; Casu, L.; Raduner, S.; Cottiglia, F.; Floris, C.; Altmann, K.-H.; Gertsch, J. Falcarinol is a covalent cannabinoid CB_1 receptor antagonist and induces pro-allergic effects in skin. *Biochem. Pharmacol.* **2010,** 79, 1815-1826.
47. Moreno, E.; Chiarlone, A.; Medrano, M.; Puigdellivol, M.; Bibic, L.; Howell, L. A.; Resel, E.; Puente, N.; Casarejos, M. J.; Perucho, J.; Botta, J.; Suelves, N.; Ciruela, F.; Gines, S.; Galve-Roperh, I.; Casado, V.; Grandes, P.; Lutz, B.; Monory, K.; Canela, E. I.; Lluis, C.; McCormick, P. J.; Guzman, M. Singular location and signaling profile of adenosine A_{2A}-cannabinoid CB_1 receptor heteromers in the dorsal striatum. *Neuropsychopharmacology* **2017**, 1-14.
48. Hudson, B. D.; Hébert, T. E.; Kelly, M. E. M. Physical and functional interaction between CB_1 cannabinoid receptors and β2-adrenoceptors. *Br. J. Pharmacol.* **2010,** 160, 627-642.
49. Hill, S. J.; May, L. T.; Kellam, B.; Woolard, J. Allosteric interactions at adenosine A_1 and A_3 receptors: new insights into the role of small molecules and receptor dimerization. *Br. J. Pharmacol.* **2014,** 171, 1102-1113.
50. May, L. T.; Bridge, L. J.; Stoddart, L. A.; Briddon, S. J.; Hill, S. J. Allosteric interactions across native adenosine-A(3) receptor homodimers: quantification using single-cell ligand-binding kinetics. *FASEB J.* **2011,** 25, 3465-3476.
51. Vauquelin, G. Determination of drug-receptor residence times by radioligand binding and functional assays: experimental strategies and physiological relevance. *MedChemComm* **2012,** 3, 645-651.
52. Sullivan, S. K.; Hoare, S. R. J.; Fleck, B. A.; Zhu, Y.-F.; Heise, C. E.; Struthers, R. S.; Crowe, P. D. Kinetics of nonpeptide antagonist binding to the human gonadotropin-releasing hormone receptor: Implications for structure–activity relationships and insurmountable antagonism. *Biochem. Pharmacol.* **2006,** 72, 838-849.

53. Ahn, K. H.; Mahmoud, M. M.; Kendall, D. A. Allosteric modulator ORG27569 induces CB_1 cannabinoid receptor high affinity agonist binding state, receptor internalization, and Gi protein-independent ERK1/2 kinase activation. *J. Biol. Chem.* **2012,** 287, 12070-12082.
54. Horswill, J. G.; Bali, U.; Shaaban, S.; Keily, J. F.; Jeevaratnam, P.; Babbs, A. J.; Reynet, C.; Wong Kai In, P. PSNCBAM-1, a novel allosteric antagonist at cannabinoid CB_1 receptors with hypophagic effects in rats. *Br. J. Pharmacol.* **2007,** 152, 805-814.
55. Colquhoun, D. Why the Schild method is better than Schild realised. *Trends Pharmacol. Sci.* **2007,** 28, 608-614.
56. Reggio, P. H. Endocannabinoid Binding to the Cannabinoid Receptors: What Is Known and What Remains Unknown. *Curr. Med. Chem.* **2010,** 17, 1468-1486.
57. Fowler, C. J.; Doherty, P.; Alexander, S. P. H. Chapter Two - Endocannabinoid Turnover. In *Advances in Pharmacology*, Kendall, D.; Alexander, S. P. H., Eds. Academic Press: 2017; Vol. 80, pp 31-66.
58. Kenakin, T. Orthosteric Drug Antagonism. In *A Pharmacology Primer: Techniques for More Effective and Strategic Drug Discovery (4th Edition)*. Academic Press: 2014; pp 128-131.
59. Rinaldi-Carmona, M.; Barth, F.; Héaulme, M.; Alonso, R.; Shire, D.; Congy, C.; Soubrié, P.; Brelière, J.-C.; Le Fur, G. Biochemical and pharmacological characterisatioN OF SR141716A, the first potent and selective brain cannabinoid receptor antagonist. *Life Sci.* **1995,** 56, 1941-1947.
60. McGuinness, D.; Malikzay, A.; Visconti, R.; Lin, K.; Bayne, M.; Monsma, F.; Lunn, C. A. Characterizing Cannabinoid CB_2 Receptor Ligands Using DiscoveRx PathHunter™ β-Arrestin Assay. *J. Biomol. Screening* **2008,** 14, 49-58.
61. Herkenham, M.; Lynn, A. B.; Little, M. D.; Johnson, M. R.; Melvin, L. S.; de Costa, B. R.; Rice, K. C. Cannabinoid receptor localization in brain. *Proc. Natl. Acad. Sci. U. S. A.* **1990,** 87, 1932-1936.
62. Miller, L. K.; Devi, L. A. The Highs and Lows of Cannabinoid Receptor Expression in Disease: Mechanisms and Their Therapeutic Implications. *Pharmacol. Rev.* **2011,** 63, 461-470.
63. Pertwee, R. G. Inverse agonism and neutral antagonism at cannabinoid CB_1 receptors. *Life Sci.* **2005,** 76, 1307-1324.
64. Erdozain, A. M.; Diez-Alarcia, R.; Meana, J. J.; Callado, L. F. The inverse agonist effect of rimonabant on G protein activation is not mediated by the cannabinoid CB_1 receptor: evidence from postmortem human brain. *Biochem. Pharmacol.* **2012,** 83, 260-268.
65. Turu, G.; Hunyady, L. Signal transduction of the CB_1 cannabinoid receptor. *J. Mol. Endocrinol.* **2010,** 44, 75-85.
66. Nogueras-Ortiz, C.; Yudowski, G. A. The multiple waves of cannabinoid 1 receptor signaling. *Mol. Pharmacol.* **2016,** 90, 620-626.